JOURNAL OF PETROLOGY | VOLUME 53 | NUMBER 11 | PAGES 2349–2379 | 2012 | doi:10.1093/petrology/egs053

Petrogenesis of Mafic to Felsic Lavas from the Oligocene Siebengebirge Volcanic Field (Germany): Implications for the Origin of Intracontinental Volcanism in Central Europe

MELANIE KOLB[1,2]*, HOLGER PAULICK[1,3], MARIA KIRCHENBAUR[1,4] AND CARSTEN MÜNKER[1,4,5]

[1]STEINMANN-INSTITUT, UNIVERSITÄT BONN, POPPELSDORFER SCHLOSS, 53115 BONN, GERMANY

[2]OMYA DEVELOPMENT AG, BASLERSTRASSE 42, 4665 OFTRINGEN, SWITZERLAND

[3]BOLIDEN MINERAL AB, KONTORSVÄGEN 1, 93632 BOLIDEN, SWEDEN

[4]UNIVERSITÄT ZU KÖLN, INSTITUT FÜR GEOLOGIE UND MINERALOGIE, ZÜLPICHER STR. 49A/B, 50674 KÖLN, GERMANY

[5]INSTITUT FÜR MINERALOGIE, UNIVERSITÄT MÜNSTER, CORRENSSTRASSE 24, 48149 MÜNSTER, GERMANY

RECEIVED JUNE 27, 2011; ACCEPTED JULY 11, 2012
ADVANCE ACCESS PUBLICATION SEPTEMBER 2, 2012

Magmatism in the Cenozoic Central European Volcanic Province (CEVP) has been related to two geodynamic scenarios, either extensional tectonics in the north Alpine realm or upwelling of deep mantle material. The Oligocene (~30–19 Ma) Siebengebirge Volcanic Field (SVF) is a major part of the German portion of the CEVP and consists of erosional remnants of mafic to felsic volcanic edifices. It covers an area of ~35 km (NW–SE) by ~25 km (SW–NE) with eruptive centres concentrated near the eastern shore of the Rhine river in the vicinity of the city of Bonn. Mafic rocks in the SVF comprise strongly SiO_2-undersaturated basanites to alkaline basalts. Occurrences of alkaline basalts are confined to an inner NW–SE-striking zone, whereas the more SiO_2-undersaturated basanites dominate the western and eastern periphery of the SVF. Radiogenic isotope compositions ($^{87}Sr/^{86}Sr$ 0·70335–0·70371; εNd +3·1 to +4·5; εHf +6·5 to +8·0; $^{206}Pb/^{204}Pb$ 19·46–19·69; $^{207}Pb/^{204}Pb$ 15·63–15·66; $^{208}Pb/^{204}Pb$ 39·34–39·62) indicate a common asthenospheric mantle end-member with HIMU-like characteristics for all mafic rocks, similar to the European Asthenospheric Reservoir (EAR). A lithospheric mantle source component with a residual K-bearing phase (phlogopite or amphibole) is inferred from negative K anomalies. Incompatible trace element modelling indicates that melting took place in the spinel–garnet transition zone with low degrees of melting at higher pressures generating the basanitic magmas ($La_N/Yb_N = 20–25$), whereas the alkaline basalts ($La_N/Yb_N = 14–18$) are the result of higher melting degrees at shallower average melting depths. Differentiation of basanitic primary melts generated tephritic to tephriphonolitic magmas that, for instance, erupted at the Löwenburg Volcanic Complex in the central SVF. Latites and trachytes, such as the prominent Drachenfels and Wolkenburg protrusions, are more common in the central portion of the SVF. These compositions originate from parental alkaline basaltic melts. All differentiated samples show evidence for crustal contamination, possibly with lower- to mid-crustal material comprising mafic granulites as found in Eifel basalt xenoliths and metapelites. Based on the spatial and temporal distribution of the various volcanic rock types, a model for the temporal evolution of the SVF can be proposed. During the initial phase of volcanism, low-degree basanitic melts were generated as a result of decompression following tectonic rifting and formation of the Cologne Embayment, a northward extension of the Rhine Graben. In a second stage, alkali basalts were generated at shallower depths and higher degrees of melting as a result of continued lithospheric thinning and passive upwelling of asthenospheric mantle. These conclusions strengthen previous models suggesting

*Corresponding author. E-mail: melanie.kolb@gmx.ch

that intraplate volcanism in Central Europe is directly linked to regional lithospheric thinning and asthenospheric upwelling. Overall, the SVF constitutes an exceptionally well-preserved magmatic assemblage to illustrate these tectono-magmatic relationships.

KEY WORDS: *intracontinental volcanism; isotope geochemistry; Central European Volcanic Province; igneous petrogenesis*

INTRODUCTION

The Siebengebirge Volcanic Field (SVF) is a prominent example of intracontinental volcanism north of the Alpine orogenic belt and forms part of the Central European Volcanic Province (CEVP). Mafic magmas with variable degrees of SiO_2-undersaturation, ranging from basanites to alkali basalts, and associated differentiated magmas (trachybasalts to tephriphonolites and latites to trachytes) were erupted from ~30 Ma to 19 Ma (Frechen & Vieten, 1970*a*, 1970*b*; Todt & Lippolt, 1980; Vieten *et al.*, 1988). In contrast to other Cenozoic volcanic provinces in Central Germany, such as the Eifel, Rhön, Vogelsberg, Westerwald, and Eger Rift complexes (Jung & Hoernes, 2000; Blusztajn & Hegner, 2002; Bogaard & Wörner, 2003; Haase *et al.*, 2004; Jung, S., *et al.*, 2005, 2011; Jung, C., *et al.*, 2006; Fekiacova *et al.*, 2007*a*, 2007*b*; Haase & Renno, 2008) the SVF is still poorly studied and the petrogenetic processes controlling the unusually diverse magmatic compositions are not fully understood.

The cause of intracontinental volcanism in Central Europe is a matter of continuing debate and various models have been proposed. Tomographic data presented by Ritter *et al.* (2001) indicate a low-velocity anomaly (LVA) beneath the Quaternary volcanic field of the Eifel, of ~100 km width and extending from 50–60 km to at least 400 km depth. This LVA was subsequently interpreted to reflect elevated temperatures of 150–200 K compared with the ambient mantle. Ritter *et al.* (2001) furthermore suggested that the currently known, finger-like European upper mantle plumes, which include the Eifel and the French Massif Central (Granet *et al.*, 1995), might have a common source in a lower mantle anomaly (~2000 km deep) as proposed by Goes *et al.* (1999). However, this view has been challenged by more recent investigations, which infer passive, diapiric instabilities in the upper mantle as the source for the intermittent Cenozoic volcanism in the entire circum-Mediterranean region (e.g. Lustrino & Wilson, 2007).

Various models have also been proposed for the mantle sources involved in CEVP magmatism, including both lithospheric and asthenospheric components (e.g. Wilson & Downes, 1991). A common asthenospheric source for the CEVP primary magmas is characterized by radiogenic Pb isotope ($^{206}Pb/^{204}Pb = 19{\cdot}6–20{\cdot}1$) and rather unradiogenic $^{87}Sr/^{86}Sr$ (0·7032–0·7034) and radiogenic $^{143}Nd/^{144}Nd$ (0·5129–0·5130). This mantle component has been termed 'component A' (Wilson & Downes, 1991), 'European Asthenospheric Reservoir' (EAR; Cebriá & Wilson, 1995; Granet *et al.*, 1995), 'Low-Velocity Component' (Hoernle *et al.*, 1995) or 'Common Mantle Reservoir' (Lustrino & Wilson, 2007). In a recent review, Lustrino (2011) emphasized the geochemical similarities of the 'anorogenic' basalts of the circum-Mediterranean intraplate volcanic province and proposed the existence of a homogeneous sub-lithospheric mantle with domains of non-peridotitic 'exotic' lithologies including remnants of oceanic crust, pyroxenite or eclogite. In general, a HIMU-like Pb isotope signature may be an indication of the presence of recycled oceanic crust (Hofmann & White, 1982) and for the CEVP it has been suggested that subducted Variscan oceanic lithosphere could have been locally incorporated into the asthenospheric mantle (Cebriá & Wilson, 1995; Hoernle *et al.*, 1995). The observed variations in the radiogenic isotope compositions of the CEVP magmas may be explained by a model in which partial melts within mantle plumes originating from an EAR-like source are mixed on a regional scale with melts from compositionally variable lithospheric mantle domains (Hoernle *et al.*, 1995; Wilson & Downes, 2006). Whether melting of the asthenospheric mantle is a result of actively rising mantle plumes or passive upwelling and lithospheric thinning is a matter of debate. In fact, both models may be applicable on a regional scale for Central European volcanism, depending on the particular characteristics of the various volcanic fields.

In addition to the role of the asthenospheric mantle, the importance of metasomatic processes in the lithospheric mantle, resulting in the formation of hydrous phases such as phlogopite and amphibole, has been emphasized in several studies (Wörner *et al.*, 1986; Wilson & Downes, 1991; Wedepohl *et al.*, 1994; Hegner *et al.*, 1995; Jung *et al.*, 2005). This concept is also supported by investigations on mantle xenoliths showing evidence for fluid- and melt-related peridotite metasomatism (Hartmann & Wedepohl, 1990; Witt-Eickschen *et al.*, 1998, 2003). Clearly, such refertilized, hydrous mantle material would readily undergo decompressional partial melting, being characterized by a relatively low solidus temperature (e.g. Anderson, 2011).

In this study we provide a comprehensive dataset for the volcanic rocks of the SVF including major and trace element concentrations obtained by X-ray fluorescence (XRF) and quadrupole inductively coupled plasma mass spectrometry (ICP-MS) as well as Sr–Nd–Hf–Pb isotope compositions. The isotope data are compared with those for other Central European volcanic provinces and are used to characterize the mantle source beneath the SVF and to constrain a possible genetic model for the evolution of the SVF magmas. In addition, the petrogenesis of the differentiated, in part silica-saturated felsic magmas in the SVF is

examined by modeling the relative contributions of differentiation processes and interaction of the magmas with the local continental crust.

GEOLOGICAL SETTING

The SVF belongs to a prominent group of Cenozoic intraplate volcanic fields in Germany, including the Hocheifel, Westerwald, Vogelsberg, Rhön, Urach–Hegau, and the Hessian Depression (Fig. 1). These volcanic fields are associated with the middle and upper Rhine rift system, which formed during Eocene to Oligocene times as a result of syn- to post-Alpine extension (Ziegler, 1992). Farther to the east, the Cenozoic volcanic rocks of the Eger Rift extend the CEVP into the Czech Republic and Poland (e.g. Haase & Renno, 2008; Ulrych *et al.*, 2011).

The SVF, Hocheifel, and Westerwald volcanic complexes are located on the Rhenish Shield, which represents a major Paleozoic tectonic block formed during the Variscan orogeny as part of the Rhenohercynian Suture Zone (e.g. Oncken *et al.*, 1999). Beneath the SVF, the basement comprises folded and weakly metamorphosed Lower Devonian sandstones and siltstones. Lower crustal xenoliths entrained in the volcanic rocks from the adjacent Eifel volcanic field include felsic to mafic granulites as well as metatonalites and metasediments (Stosch & Lugmair, 1984, 1986; Loock *et al.*, 1990; Rudnick & Goldstein, 1990; Stosch *et al.*, 1991). The crustal thickness is estimated to be less than 30 km (Prodehl, 1981; Prodehl *et al.*, 1992) and the present-day lithosphere–asthenosphere boundary is located at a depth of ~80 km (Babuska & Plomerova, 1992).

The SVF is located close to the southeastern limit of the Cologne Embayment, a regional zone of tectonic subsidence encroaching on the Rhenish Shield since the Oligocene (Fig. 1). The volcanic rocks occur in an area some 35 km (NW–SE) by 25 km (SW–NE) and their regional distribution defines NW–SE-trending alignments normal to the direction of extensional stress and parallel to the orientation of the Rhine river and normal faults in the area (Fig. 1b). The post-volcanic erosion was substantial, owing to the uplift of the Rhenish Shield, and most of the volcanic rocks now exposed represent the sub-volcanic root zones of volcanic edifices.

The centre of the SVF is located on the eastern side of the Rhine river close to the city of Bonn (Fig. 1a). In this central zone, known as the Siebengebirge in a geographical sense, a diversity of volcanic rock types occurs. The more differentiated SVF lavas (latites and trachytes) are abundantly found restricted to the central part of the SVF in an area of ~10 km^2. However, the Löwenburg Volcanic Complex (LVC), in the eastern portion of the central SVF, consists of SiO_2-undersaturated rocks ranging from trachybasalt to tephriphonolite (Figs 1b and 2). Overall, the magmas of the SVF span an exceptionally large range in terms of SiO_2-undersaturation, which has been highlighted by previous workers (Frechen & Vieten, 1970*a*, 1970*b*; Vieten, 1983, 1987; Vieten *et al.*, 1988). In the TAS (total alkalis–silica) classification diagram (Fig. 2; Le Maitre, 2002), the compositions of the mafic volcanic rocks, which are volumetrically dominant in the SVF, define a continuous range from basanite to alkali basalts, whereas the more evolved compositions range from latite to trachyte.

The age of Siebengebirge volcanism has been constrained by K–Ar dating of lava samples from 20 localities in the centre and periphery of the volcanic field as reported by Todt & Lippolt (1980; Fig. 1c). In addition, two basanite occurrences have been recently dated using the ^{40}Ar–^{39}Ar method (Linthout *et al.*, 2009). Moreover, separates of sanidine megacrysts from the Drachenfels trachyte (sample DRA-1; locality labeled 'A' in Fig. 1b) are being used as an internal standard at the Ar–Ar laboratory at the Vrije Universitet Amsterdam (J. Wijbrans, personal communication). The data show that the trachytes and latites were erupted mainly between ~27 and ~25 Ma. Tephriphonolites from the LVC exhibit a similar age range (~26 to ~24 Ma). In contrast, the mafic rocks erupted over a considerably longer time span from ~30 Ma to ~19 Ma. Importantly, the age data suggest that there has been a temporal shift in the degree of SiO_2-saturation of the erupted mafic magmas. Older ages (~30 to ~24 Ma) are restricted to basanite samples, whereas alkaline basalts are mainly younger, ranging from ~25 to ~19 Ma in age.

SAMPLING APPROACH AND ANALYTICAL METHODS

Based on a compilation of previous data for SVF lavas (Frechen & Vieten, 1970*a*, 1970*b*; Metzner, 1983; Vieten, 1987; Vieten *et al.*, 1988) we re-sampled 28 representative sites in the SVF (Table 1). The material was crushed in a steel jaw crusher and subsequently examined under a binocular microscope to remove any alteration rims and xenoliths prior to grinding in an agate mill. Also included were three powder samples from the collection of K. Vieten from outcrops that are no longer accessible (samples SG 13, SG 17, SG 21). These 31 samples cover the entire compositional range and areal extent of the SVF (Electronic Appendix, available for downloading at http://www.oxfordjournals.org; see also Fig. 1).

Major element compositions and concentrations of Co, Cr, Nb, Ni, Rb, Sr, V, and Zr were analyzed by XRF using a Philips PW-1480 spectrometer at the Universität Bonn, Germany. Normative mineral abundances were calculated using the PetroGraph software applying the CIPW protocol (Petrelli *et al.*, 2005). We selected 22 samples for detailed trace element analysis by quadrupole

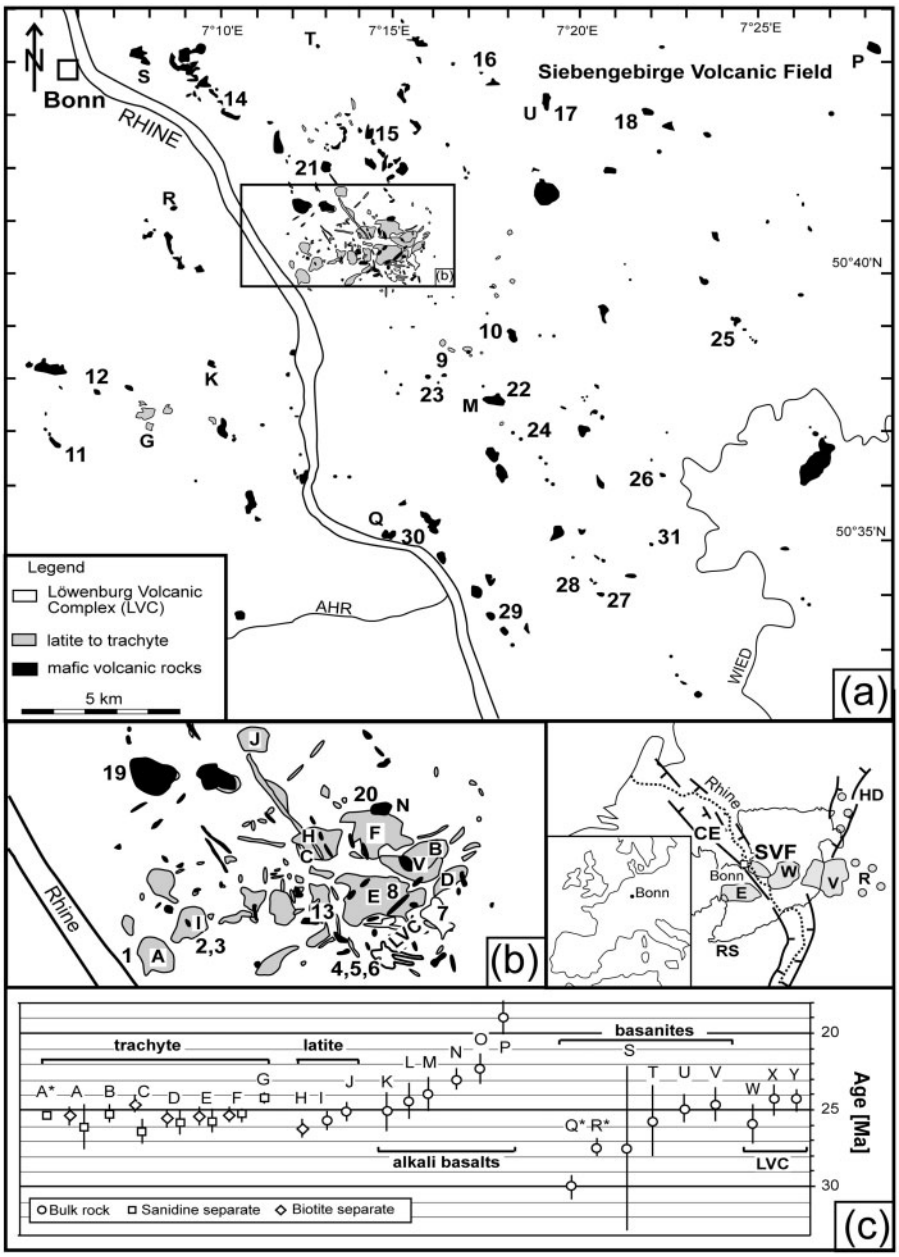

Fig. 1. (a, b) Maps of the Siebengebirge Volcanic Field (SVF) (numbers indicate samples from this study; letters indicate locations with radiometric age determinations, literature data). The maps were compiled from the following 1:25 000 scale geological maps published by the Geological Surveys of Rheinland–Pfalz and Nordrhein-Westfalen: 5208 (Bonn), 5209 (Siegburg), 5210 (Eitorf), 5308 (Bad Godesberg), 5309 (Königswinter), 5310 (Asbach), 5408 (Bad Neuenahr–Ahrweiler), 5409 (Linz), 5410 (Waldbreitbach), 5509 (Burgbrohl). The inset map shows the distribution of Cenozoic volcanic fields in central Germany. CE, Cologne Embayment; E, Eifel (including the Paleogene Hocheifel and the Quaternary East and West Eifel volcanic fields); HD, Hessian depression; R, Rhön; RS, Rhenish Shield; SVF, Siebengebirge Volcanic Field; W, Westerwald. The extent of the Paleozoic Rhenish Shield is indicated with a thin, solid line. (c) Summary of available age data for the SVF rocks (error bars are 2σ RSD). Ages were determined by the K–Ar method (Todt & Lippolt, 1980) except for data marked with an asterisk, representing Ar–Ar dating (Linthout *et al.*, 2009; J. Wijbrans, personal communication). Location code: A and A*, Drachenfels; B, Lahrberg, C, Wasserfall; D, Perlenhardt; E, Lohrberg; F, Ölberg trachyte; G, Hohenberg–Berkum, Domsteinbruch; H, Rosenau; I, Wolkenburg; J, Stenzelberg; K, Dächelsberg; L, Kahlenberg [not shown in (b), located south of the map area close to the Brohl river]; M, Asberg; N, Ölberg basalt; O, Steinbergskopf [not shown in (b), located south of the map area close to the Brohl river]; P, Stein–Eitorf; Q*, top of Erpeler Ley; R*, Godesburg; S, Finkenberg; T, Stieldorf 1 drill core depth 81 m; U, Stuxenberg; V, Hardt, East Margarethenhöhe; W, X, Y, Löwenburg.

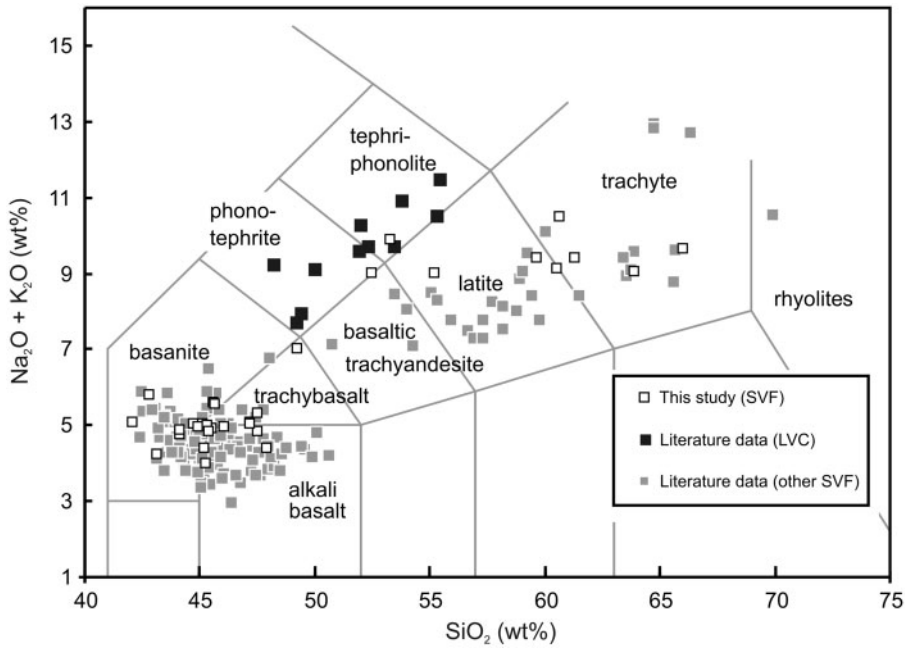

Fig. 2. Total alkalis–silica (TAS) classification diagram for the SVF rocks (Le Maitre, 2002). Major element data are normalized to 100% anhydrous. The field for trachyandesite is labeled here 'latite', as all samples display $K_2O \geq (Na_2O - 2)$ as defined by Le Maitre (2002). Literature data are compiled from several sources outlined in the Electronic Appendix.

ICP-MS at Universität Kiel, Germany, using an Agilent 7500cs instrument following the procedures outlined by Garbe-Schönberg (1993). The external reproducibility for trace element analyses is of the order of ±5 to ±10% and measurements of the BHVO-1 standard were within 10% of the recommended literature values (Govindaraju, 1994).

Sr–Nd–Hf isotope compositions were determined for 14 mafic and eight differentiated samples at Universität Münster, Germany, using ~100 mg of leached rock powder. For the Drachenfels trachyte (sample SG 1) the $^{87}Sr/^{86}Sr$ composition was also determined for hand-picked sanidine megacrysts. Hafnium was separated using the one column Eichrom Ln-Spec resin procedure of Münker *et al.* (2001). Strontium and Nd were separated from the remaining matrix using conventional ion exchange techniques. The Sr and Nd isotope compositions were analyzed by thermal ionization mass spectrometry (TIMS) on a Thermo-Finnigan Triton system operated in static mode. Repeated measurements of the La Jolla standard gave a $^{143}Nd/^{144}Nd$ of $0{\cdot}511826 \pm 0{\cdot}000011$ (2σ) with long-term external reproducibility of ±30 ppm. For Sr isotope analyses, a long-term external reproducibility of ±40 ppm is achieved. Repeated runs of the NBS 987 standard yielded an $^{87}Sr/^{86}Sr$ of $0{\cdot}710262 \pm 0{\cdot}000014$ (2σ). Hafnium and Pb isotope analyses were performed by multi-collector (MC)-ICP-MS (using a Micromass IsoProbe system) at Universität Münster. Measurements of the Münster AMES Hf-standard, which is isotopically indistinguishable from the JMC-475 standard, gave an average value of 0·282146 with a long-term reproducibility of ±50 ppm. All Hf results are given relative to a value of 0·282160. The εHf and εNd values were calculated using CHUR values of $^{176}Hf/^{177}Hf = 0{\cdot}282772$ (Blichert-Toft & Albarède, 1997) and $^{143}Nd/^{144}Nd = 0{\cdot}512638$ (Wasserburg *et al.*, 1981). Lead isotope compositions were obtained for nine mafic samples following the procedure of Schuth *et al.* (2011). Small rock chips (~250 mg) were cleaned using ultrasound in de-ionized H_2O and leached for 1 h in hot 6N HCl and 3N HCl, respectively. Lead was then separated from the matrix employing an HCl–HBr procedure, which was repeated once to ensure that a clean Pb fraction was obtained (e.g. Korkisch & Hazan, 1965). Lead isotope analyses by MC-ICP-MS were corrected for mass fractionation by addition of the Tl standard NBS 997 prior to measurement (see, e.g. Hirata, 1996; Rehkämper & Halliday, 1998; Albarède *et al.*, 2004; Schuth *et al.*, 2011) and are given relative to the NBS 981 values of Galer & Abouchami (1998). Our results for the NBS 981 standard average 16·929 for $^{206}Pb/^{204}Pb$, 15·486 for $^{207}Pb/^{204}Pb$ and 36·685 for $^{208}Pb/^{204}Pb$. The 2SD errors were ±126 ppm for $^{206}Pb/^{204}Pb$, ±183 ppm for $^{207}Pb/^{204}Pb$ and ±193 ppm for $^{208}Pb/^{204}Pb$. All geochemical data obtained during this study together with previous SVF data are compiled in the Electronic Appendix. Representative major and trace element analyses are presented along with the isotope data in Tables 2 and 3.

RESULTS

Petrography

Field relationships indicate that the samples mostly represent sub-volcanic, shallow intrusive rocks and the remains of magmatic feeder systems. This is also reflected in the petrographic characteristics, as the groundmass is generally microcrystalline with variable proportions of phenocrysts (Table 1). The mafic samples contain olivine and clinopyroxene phenocrysts (Ti-augite and green-core pyroxenes; Duda & Schmincke, 1985) and minor plagioclase.

The latites and trachytes mainly contain sanidine, plagioclase, amphibole, clinopyroxene, biotite, and minor titanite phenocrysts. One sample (SG 1; Drachenfels trachyte) contains exceptionally large sanidine megacrysts up to 7 cm in size.

The phonotephrites to tephriphonolites from the LVC contain clinopyroxene, amphibole and minor plagioclase phenocrysts. Olivine-rich xenoliths are present in some of the mafic samples (Table 1). Furthermore, xenoliths of crustal origin (gneiss fragments, quartz and feldspar xenocrysts, siltstone fragments) are locally present in both mafic and felsic samples.

Geochemistry

Major and trace element geochemistry

The major and trace element compositions of the 31 analyzed samples are reported in Tables 2 and 3 and the Electronic Appendix. The SVF hosts a large variety of volcanic rock types, both in terms of degree of differentiation and with respect to the level of SiO_2-saturation. Figure 2 shows the classification of all the studied samples in a total alkalis–silica diagram (TAS, after Le Maitre, 2002). According to IUGS classification rules, most of the mafic samples are classified as Ne-normative basanites, tephrites, and alkali basalts, with various degrees of silica-undersaturation. In contrast, the two samples SG 15 (Scharfenberg) and SG 24 (Kiezhaus) are silica-saturated (hypersthene-normative) and are therefore classified as subalkaline basalt and hawaiite, respectively. The more differentiated rock types include one phonotephrite (SG 6), one tephriphonolite (SG 7), three latites (SG 3, SG 8, and SG 9; corresponding to a K-rich trachyandesite) as well as four trachyte samples (SG 1, SG 2, SG 5, SG 10).

Variations in the normative nepheline content reveal that there is a distinctive zonation within the SVF (Fig. 3). A NW–SE-trending central zone is dominated by alkali basalts with low normative nepheline contents (<2%) and is flanked to the SW and NE by basanitic volcanic centres with elevated amounts of normative nepheline (2% to >5%; maximum 12·5%). The LVC represents the most notable exception from this general pattern, exhibiting strongly SiO_2-undersaturated magmas in the central Siebengebirge (normative nepheline up to 18·5%). Amongst the more differentiated lavas, phonotephritic to tephriphonolitic compositions are restricted to the LVC whereas latites and trachytes are abundant in the central SVF and also occur locally in the peripheral area (e.g. west of the Rhine river, Fig. 1a).

The major element variations of the SVF samples follow typical differentiation trends that are consistent with the observed phenocryst assemblages. Decreasing concentrations of MgO (Fig. 4a) and Fe_2O_{3total} (not shown) with increasing SiO_2 are related to the fractionation of olivine and clinopyroxene. Likewise, decreasing Ni and Sc concentrations with decreasing MgO (Fig. 4e and f) can be linked to the fractionation of olivine and clinopyroxene. A decrease of CaO with SiO_2 (not shown) is also partially controlled by clinopyroxene fractionation. Concentrations of Al_2O_3 increase until a SiO_2 content of ~55 wt % is reached (Fig. 4b), indicating that the initial differentiation of the mafic magmas is occurring at conditions above the solidus for plagioclase. Likewise, the tephriphonolite and phonotephrite samples from the LVC (51·8 and 53·4 wt % SiO_2) exhibit a general increase in Al_2O_3. SVF samples with SiO_2 contents above 55 wt % show slightly decreasing Al_2O_3 concentrations (~18 to ~16 wt %) and decreasing Sr contents with increasing SiO_2 (Fig. 4g).

Decreasing concentrations of TiO_2 with increasing degree of differentiation are probably related to the combined effect of fractionating Ti-augite, titanite and ilmenite (Fig. 4c), and fractionation of apatite is reflected in decreasing P_2O_5 concentrations (not shown). Figure 4d shows that K_2O is successively enriched in the magma during the course of differentiation, which is remarkable as sanidine is a common phenocryst phase in the latite and trachyte samples. Compared with the latites and trachytes, the tephriphonolites and phonotephrites from the LVC are characterized by higher K_2O at similar SiO_2 contents.

The SVF volcanic rocks are light rare earth element (LREE)-enriched with similar smooth chondrite-normalized patterns for basanites, alkali basalts, phonotephrites–tephriphonolites and latite–trachyte samples (Fig. 5a–d). In general, the basanite samples ($La_N/Yb_N = 18–27$) are slightly more LREE-enriched than the alkali basalts ($La_N/Yb_N = 15–20$; Fig. 5e).

The differentiated SVF lavas (latites, trachytes, phonotephrites, and tephriphonolites) are more LREE-enriched than the mafic samples ($La_N = 300–400$ compared with 150–300) at similar heavy rare earth element (HREE) contents. A negative Eu anomaly (0·83 and 0·88; see Table 3) is developed only in two trachytes (SG 1 and SG 2). Importantly, the phonotephrite and tephriphonolite samples have higher La_N/Yb_N ratios (30–45) than the latite–trachyte samples (20–28). In the La_N/Yb_N–SiO_2 diagram (Fig. 5e) two diverging trends are evident: a high La_N/Yb_N trend defined by basanitic to tephriphonolitic

Table 1: Sample localities and petrographic characteristics of the SVF lavas

Sample	Rock type	Location	Description	Latitude (N)	Longitude (E)
SG 1	Trachyte	Drachenfels	Coarsely porphyritic trachyte, 20% sanidine megacrysts (up to 7 cm), phen ≤1 cm (~15%): plag, cpx, bt, and ttn	50·666	7·206
SG 2	Trachyte	Wolkenburg	Strongly porphyritic trachyte, ~35% phen of plag, san, amp, cpx, and bt. Crustal xenoliths (gneiss)	50·665	7·214
SG 3	Latite	Wolkenburg	Strongly porphyritic latite, ~40% phen of plag, san, amp, cpx, and bt	50·666	7·212
SG 4	Tephrite	Löwenburg	Tephrite with intersertal texture. Zoned cpx (30%), plag (20%), and ol (5%)	50·663	7·25
SG 5	Trachyte	Löwenburg	Strongly porphyritic trachyte dike. ~30% phen of san, plag, cpx and amp. Abundant crustal xenoliths (shale and siltstone)	50·662	7·251
SG 6	Phonotephrite	Löwenburg	Porphyritic phonotephrite, ~20% phen of cpx, zoned amp, and plag	50·662	7·252
SG 7	Tephriphonolite	Scheerkopf	Flow foliated tephriphonolite, ~15% phen of zoned amp, zoned cpx, and plag	50·669	7·257
SG 8	Latite	Lohrberg	Flow foliated latite, ~25% phen of plag, cpx, san, amp, bt, and ttn. Some green-core cpx	50·674	7·245
SG 9	Latite	Mittelberg	Flow foliated latite, ~30% phen of plag, zoned san, cpx, and amp	50·641	7·277
SG 10	Trachyte	Broderkonsberg	Trachyte with intersertal texture composed of plag laths. ~5% phen of cpx and amp	50·639	7·284
SG 11	Basanite	Arzdorf	Fine-grained basanite. ~30% phen of ol and zone cpx	50·610	7·098
SG 12	Basanite	Wachtberg	Fine-grained basanite. ~30% phen of cpx and ol. Some green-core cpx. Some cpx with ap inclusions. Peridotite xenoliths	50·627	7·119
SG 13	Tephrite	Gang, N Ölend	Fine-grained tephrite. ~10% phen of zoned cpx, ol and plag	50·668	7·239
SG 14	Tephrite	Kuckstein, Oberkassel	Fine-grained tephrite. ~15% phen of zoned cpx and ol. Some glomerophyric cpx clots	50·714	7·177
SG 15	Subalkaline basalt	Scharfenberg	Fine-grained subalkaline basalt ~5% phen of ol and cpx	50·707	7·238
SG 16	Tephrite	N Pleiserhohn	Fine-grained tephrite ~10% phen of ol and zoned cpx	50·728	7·29
SG 17	Tephrite	Stuxenberg	Fine-grained tephrite ~20% phen of zoned cpx and ol	50·718	7·318
SG 18	Basanite	Eulenberg	Fine-grained basanite. ~15% phen of ol and cpx. Large peridotite xenoliths	50·689	8·779
SG 19	Alkali basalt	Petersberg	Flow foliated alkali basalt. ~15% phen of ol and cpx	50·687	7·208
SG 20	Alkali basalt	Ölberg	Flow foliated alkali basalt. ~15% phen of ol and cpx	50·683	7·249
SG 21	Basanite	Groβer Weilberg	Fine-grained basanite. ~30% phen of ol and cpx. Some glomerophyric cpx clots	50·698	7·219
SG 22	Basanite	Asberg	Fine-grained basanite. ~30% phen of ol and cpx. Some glomerophyric cpx clots	50·625	7·299
SG 23	Basanite	Hasenhardt	Fine-grained basanite. ~20% phen of ol and cpx. Some green-core cpx and peridotite xenoliths	50·629	7·285
SG 24	Hawaiite	Kretzhaus	Flow foliated hawaiite. ~10% phen of ol, cpx and plag	50·615	7·305
SG 25	Tephrite	Oberplag	Fine-grained tephrite ~5% phen of cpx and ol. Some green-core cpx	50·643	7·422
SG 26	Alkali basalt	Strödter Hügel	Flow foliated alkali basalt. ~15% phen of ol, cpx and ol. Crustal xenoliths (qtz with cpx reaction rims)	50·601	7·371
SG 27	Basanite	Römerich	Flow foliated basanite. ~15% phen of cpx and ol. Green-core cpx. Crustal xenoliths (qtz with cpx reaction rims)	50·564	7·343
SG 28	Tephrite	Dattenberger Wald	Fine-grained tephrite. ~5% phen of ol and cpx. Glomerophyric cpx clots. Crustal xenoliths (qtz with cpx reaction rims)	50·569	7·339
SG 29	Basanite	Schwarzer See, E Dattenberg	Flow foliated basanite. ~15% phen of ol and cpx. Abundant microphen of plag. Crustal xenoliths (qtz with cpx reaction rims)	50·552	7·300
SG 30	Basanite	Erpeler Ley	Fine-grained basanite. ~15% phen of ol, cpx and plag. Green-core cpx. Peridotite xenoliths	50·582	7·247
SG 31	Alkali basalt	Rödderhof	Fine-grained alkali basalt. ~25% phen of ol, cpx and plag. Green-core cpx. Crustal xenoliths (qtz with cpx reaction rims)	50·579	7·362

Abbreviations for phenocrysts (phen): plag, plagioclase; san, sanidine; ol, olivine; cpx, clinopyroxene; amph, amphibole; bt, biotite; ttn, titanite.

Table 2: Major element analyses of representative samples along with the calculated normative mineral abundance using the PetroGraph software (Petrelli et al.*, 2008)*

Sample:	SG 1	SG 2	SG 5	SG 10	SG 3	SG 8	SG 9	SG 6	SG 7	SG 11
Rock type:	Trachyte	Trachyte	Trachyte	Trachyte	Latite	Latite	Latite	Phonotephrite	Tephriphonolite	Basanite
Location:	Drachenfels	Wolkenburg	Löwenburg	Broderkonsberg	Wolkenburg	Lohrberg	Mittelberg	Löwenburg	Scheerkopf	Arzdorf (reassay of sample V-34)
wt %										
SiO_2	64·7	60·7	62·8	59·3	60·3	59·1	54·5	51·8	53·4	44·7
TiO_2	0·82	1·28	0·96	1·04	1·25	1·42	1·86	1·59	1·69	2·24
Al_2O_3	16·5	17·7	16·8	18·0	17·4	17·3	18·2	16·9	17·5	13·1
Fe_2O_3total	3·58	5·00	4·42	4·20	4·84	5·48	6·33	6·39	6·78	10·6
MnO	0·09	0·16	0·13	0·12	0·12	0·17	0·18	0·15	0·15	0·19
MgO	0·75	1·00	1·36	1·61	1·63	1·49	2·31	3·90	3·66	12·2
CaO	1·85	3·55	2·80	3·04	3·76	4·48	6·11	6·18	6·67	10·4
Na_2O	4·70	4·77	4·33	5·85	4·50	5·16	4·49	5·32	6·37	3·88
K_2O	4·77	4·54	4·57	4·43	4·51	4·19	4·40	3·34	3·57	1·12
P_2O_5	0·20	0·29	0·20	0·21	0·29	0·39	0·39	0·47	0·51	0·63
LOI	1·00	0·69	0·80	1·07	1·04	0·48	0·79	2·99	0·72	0·65
Total	99·0	99·7	99·2	98·9	99·6	99·6	99·5	99·1	101·0	99·7
CaO/Al_2O_3	0·11	0·20	0·17	0·17	0·22	0·26	0·34	0·37	0·38	0·80
Mg#	32·8	31·8	41·8	47·2	43·9	38·8	46·0	58·7	55·7	72·8
Normative phases										
Albite	40·6	40·8	37·3	50·6	38·6	44·0	38·5	38·8	34·2	20·0
Anorthite	8·29	13·6	12·8	10·0	14·2	11·8	16·7	12·9	8·58	15·2
Apatite	0·48	0·7	0·48	0·50	0·70	0·92	0·94	1·16	1·19	1·49
Corundum	0·64	0	0·12	0	0	0	0	0	0	0
Diopside	0	0	0	0·49	0	3·02	4·28	8·4	12·4	20·0
Hematite	3·67	5·05	4·47	4·30	4·87	5·54	6·38	6·66	6·78	10·7
Hypersthene	1·91	2·51	3·44	3·87	4·12	2·34	0	0	0	0
Ilmenite	0·20	0·35	0·28	0·26	0·26	0·37	0·39	0·33	0·32	0·41
Leucite	0	0	0	0	0	0	0	0	0	0
Nepheline	0	0	0	0	0	0	0	4·35	10·6	7·13
Olivine	0	0	0	0	0	0	2·69	4·36	2·33	15
Orthoclase	28·8	27·1	27·5	26·8	27·0	25·0	26·3	20·5	21·0	6·68
Perovskite	0	0	0	0	0	0	0·72	2·52	2·58	3·48
Quartz	14·8	7·81	12·87	0·9	7·87	4·07	0	0	0	0
Rutile	0·73	0·39	0·83	0	0·26	0	0	0	0	0
Titanite	0	1·77	0	2·27	2·14	3·04	3·09	0	0	0

(continued)

samples, and a low La_N/Yb_N trend defined by the alkali basaltic to trachytic rocks.

In primitive mantle-normalized multi-element diagrams the basanites and alkali basalts show similar patterns with enriched incompatible element concentrations (Fig. 6). Such patterns in mafic magmas are characteristic of continental intraplate volcanism in central Europe and the circum-Mediterranean area (e.g. Lustrino & Wilson, 2007; Lustrino, 2011). The SVF mafic lavas show maxima for Ba, Th, and U as well as for Nb and Ta, whereas negative anomalies are present for Cs, K, and Pb relative to elements of similar incompatibility. A small trough at Zr and Hf is also present that is particularly well developed in the basanite samples (Fig. 6a). Anomalies of Zr_N

Table 2: Continued

Sample:	SG 13	SG 18	SG 22	SG 23	SG 27	SG 29	SG 30	SG 21	SG 4	SG 13	SG 14
Rock type:	Basanite	Basanite	Basanite	Basanite	Basanite	Basanite	Basanite	Basanite	Tephrite	Tephrite	Tephrite
Location:	Wachtberg (reassay of sample V-107)	Eulenberg	Asberg	Hasenhardt	Römerich	Schwarzer See	Erpeler Ley	Groβer Weilberg (reasssay of sample V-55)	Löwenburg	N Ölend (reassay of sample V-30.1)	Kuckstein, Oberkassel (reassay of sample V-74)
wt %											
SiO_2	42·5	44·9	45·4	45·2	43·7	44·6	44·4	44·3	48·1	43·7	44·5
TiO_2	2·68	2·34	2·42	2·45	2·83	2·46	2·67	2·08	2·38	1·96	2·23
Al_2O_3	13·1	13·1	13·7	13·4	14·0	13·5	13·8	12·7	15·4	13·8	13·8
Fe_2O_3total	11·8	10·8	11·3	11·4	12·5	11·3	11·0	12·8	9·13	10·7	10·6
MnO	0·20	0·18	0·19	0·19	0·19	0·18	0·19	0·23	0·17	0·25	0·19
MgO	11·5	12·5	10·8	10·9	9·06	11·1	10·3	10·6	6·29	8·48	9·26
CaO	11·8	10·6	10·5	10·6	11·3	10·7	10·3	10·7	8·66	11·1	10·9
Na_2O	3·41	3·66	3·97	3·66	3·39	3·02	3·83	2·70	4·34	3·26	4·55
K_2O	0·76	1·30	0·94	1·33	1·35	1·33	0·91	1·22	2·57	2·13	0·89
P_2O_5	0·76	0·65	0·54	0·56	0·76	0·52	0·53	0·48	0·69	0·55	0·58
LOI	2·19	0·71	0·64	0·46	0·47	0·70	1·22	0·30	1·59	1·73	2·89
Total	100·7	100·6	100·4	100·2	99·5	99·4	99·0	98·1	99·2	97·7	100·3
CaO/Al_2O_3	0·90	0·81	0·77	0·79	0·80	0·79	0·74	0·84	0·56	0·80	0·79
Mg#	69·3	73·1	69·0	69·1	62·9	69·6	68·6	65·8	61·6	65·0	67·1
Normative phases											
Albite	17·5	18·7	24·0	21·5	21·0	21·5	25·0	23·1	30·1	14·4	21·9
Anorthite	18·5	15·5	16·8	16·3	19·2	19·6	18·2	19·4	15·3	17·4	15·0
Apatite	1·83	1·54	1·27	1·33	1·81	1·25	1·28	1·17	1·66	1·36	1·41
Corundum	0	0	0	0	0	0	0	0	0	0	0
Diopside	21·2	19·8	18·8	19·5	18·1	17·7	16·9	19·6	12·8	23·5	22·9
Hematite	12·0	10·8	11·3	11·4	12·6	11·5	11·2	13·1	9·31	11·2	10·9
Hypersthene	0	0	0	0	0	0	0	0	0	0	0
Ilmenite	0·43	0·38	0·41	0·41	0·41	0·39	0·42	0·50	0·37	0·56	0·42
Leucite	0	0	0	0	0	0	0	0	0	0	0
Nepheline	6·4	6·62	5·22	5·21	4·29	2·36	4·36	0·16	4·04	7·79	9·53
Olivine	13·4	15·4	12·8	12·8	10·1	13·9	12·9	12·5	7·06	7·81	9·14
Orthoclase	4·56	7·68	5·57	7·88	8·05	7·96	5·49	7·37	15·5	13·1	5·39
Perovskite	4·24	3·64	3·77	3·82	4·50	3·89	4·27	3·17	3·81	2·98	3·52
Quartz	0	0	0	0	0	0	0	0	0	0	0
Rutile	0	0	0	0	0	0	0	0	0	0	0
Titanite	0	0	0	0	0	0	0	0	0	0	0

(continued)

($Zr_N/Zr_N^* = Zr_N/[\sqrt{(Sm_N \times Nd_N)}]$) and Hf_N ($Hf_N/Hf_N^* = Hf_N/[\sqrt{(Sm_N \times Nd_N)}]$) were calculated and range between 0·64 and 0·9.

The differentiated samples display broadly similar primitive mantle-normalized patterns compared with the mafic samples but there are some marked differences (Fig. 6). Importantly, a negative Pb anomaly is absent, the magnitude of the negative K anomaly is substantially reduced and there is no indication for a Zr–Hf trough. Furthermore, negative Sr and Ba anomalies are particularly pronounced in the latites and trachytes (Fig. 6b).

Sr–Nd–Hf–Pb isotope systematic

The SVF basanites and alkali basalts define overlapping and narrow compositional fields in terms of isotopic composition ($\varepsilon Nd = +3{\cdot}1$ to $+4{\cdot}5$; $\varepsilon Hf = +6{\cdot}5$ to $+8{\cdot}0$;

Table 2: Continued

Sample:	SG 16	SG 17	SG 25	SG 28	SG 31	SG 19	SG 20	SG 26	SG 24	SG 15
Rock type:	Tephrite	Tephrite	Tephrite	Tephrite	Alkali basalt	Alkali basalt	Alkali basalt	Alkali basalt	Hawaiite	Subalkaline basalt
Location:	N Pleiserhohn	Stuxenberg (reassay of sample V-96)	Oberplag	Dattenberger Wald	Rödderhof	Petersberg (reassay of sample V-31a)	Ölberg	Strödter Hügel	Kietzhaus	Scharfenberg
wt %										
SiO_2	43·6	41·0	41·9	42·9	45·2	47·2	46·8	46·8	47·4	48·1
TiO_2	2·35	2·44	3·10	3·28	2·27	2·20	2·25	2·21	2·54	2·35
Al_2O_3	12·4	12·9	14·5	15·0	14·6	14·2	14·5	14·1	15·1	14·6
Fe_2O_3total	11·1	15·0	12·1	12·9	10·7	11·3	10·3	11·2	11·1	11·4
MnO	0·19	0·27	0·21	0·19	0·19	0·19	0·18	0·19	0·17	0·18
MgO	10·3	8·83	8·00	7·24	9·30	9·06	9·33	9·30	8·18	8·71
CaO	12·2	11·2	11·6	10·1	10·7	9·97	10·5	10·0	9·38	10·3
Na_2O	4·24	3·46	4·56	3·64	3·46	3·62	3·63	3·77	3·74	3·38
K_2O	0·70	1·52	1·13	1·14	1·42	1·19	1·41	1·23	1·56	1·05
P_2O_5	0·66	0·80	0·89	0·96	0·53	0·46	0·46	0·53	0·52	0·43
LOI	2·50	1·31	1·65	1·10	1·01	0·42	0·45	0·63	0·49	0·53
Total	100·1	98·7	99·5	98·5	99·3	99·8	99·8	100·0	100·2	100·9
CaO/Al_2O_3	0·98	0·87	0·80	0·67	0·73	0·70	0·72	0·71	0·62	0·70
Mg#	68·4	57·9	60·7	56·7	64·1	67·0	65·1	67·8	65·9	63·2
Normative phases										
Albite	17·5	14·2	16·8	29·3	22·6	30·7	25·8	29·0	31·7	28·5
Anorthite	13·0	15·6	16·1	21·8	20·5	19·1	19·2	18·0	19·9	21·5
Apatite	1·59	1·94	2·15	2·33	1·26	1·09	1·1	1·25	1·24	1·02
Corundum	0	0	0	0	0	0	0	0	0	0
Diopside	28·7	22·2	20·7	9·55	17·7	16·2	17·9	16·7	11·9	14·9
Hematite	11·4	15·4	12·4	13·3	10·9	11·4	10·4	11·3	11·1	11·3
Hypersthene	0	0	0	0	0	0	0	0	0	2·56
Ilmenite	0·42	0·59	0·46	0·42	0·41	0·41	0·39	0·41	0·36	0·38
Leucite	0	0	0	0	0	0	0	0	0	0
Nepheline	10·4	8·57	12·2	1·3	3·88	0·09	2·75	1·68	0	0
Olivine	9·04	8·62	7·54	9·88	10·8	10·6	10·6	10·9	10·5	8·49
Orthoclase	4·23	9·22	6·81	6·92	8·53	7·07	8·39	7·32	9·25	6·17
Perovskite	3·72	3·73	4·98	5·36	3·56	3·4	3·51	3·42	3·8	0
Quartz	0	0	0	0	0	0	0	0	0	0
Rutile	0	0	0	0	0	0	0	0	0	0
Titanite	0	0	0	0	0	0	0	0	0·3	5·24

LOI, loss on ignition.

$^{87}Sr/^{86}Sr = 0{\cdot}703352–0{\cdot}703714$; $^{206}Pb/^{204}Pb = 19{\cdot}46–19{\cdot}69$; $^{207}Pb/^{204}Pb = 15{\cdot}63–15{\cdot}66$; $^{208}Pb/^{204}Pb = 39{\cdot}34–39{\cdot}62$; Table 3). These ranges of Sr–Nd–Hf–Pb isotope compositions are characteristic for mafic intraplate magmas as found throughout the CEVP (Lustrino & Wilson, 2007).

In Sr–Nd isotope space (Fig. 7a) the mafic SVF samples plot close to the field defined for the European Asthenospheric Reservoir (EAR; Cebriá & Wilson, 1995), proposed to represent a common depleted end-member for the CEVP range of compositions. If only mafic SVF samples with more than 7 wt % MgO are considered, they still overlap the field defined for similarly mafic CEVP magmas (Fig. 7a). More radiogenic $^{87}Sr/^{86}Sr$ isotope compositions than in the SVF were previously

Table 3: Trace element concentrations obtained by quadrupole ICP-MS and Sr–Nd–Hf–Pb isotope compositions

Sample code:	SG	JW	SG	SG	SG	SG	SG	SG
Sample no.:	1	DRA-1	2	5	10	3	8	9
Rock type:	Trachyte	Sanidine	Trachyte	Trachyte	Trachyte	Latite	Latite	Latite
Location:	Drachenfels	Drachenfels	Wolkenburg	Löwenburg	Broderkonsberg	Wolkenburg	Lohrberg	Mittelberg
Trace elements (ppm)								
Ba	505		960	*864*	*914*	*776*	*716*	922
Co	5·90		9·50					14·4
Cr	4·00		6·00	*38*	*18*	*3*	*3*	10·0
Cs	2·43		2·07					1·77
Cu	5·30		12·5					12·1
Ga	25·6		25·9					26·0
Hf	2·47		2·31					9·04
Li	33·8		23·0					26·9
Mo	0·790		2·67					5·05
Nb	69·6		86·3	*81*	*98*	*81*	*60*	100
Ni	*36*		*53*	*73*	*18*	*10*	*11*	6·00
Pb	10·9		15·0					11·0
Rb	184		155	*150*	*120*	*76*	*158*	126
Sb	0·117		0·156					0·211
Sc	4·10		7·00	*12*	*5*	*6*	*2*	8·30
Sr	365		700	*589*	*1036*	*1007*	*447*	864
Ta	3·59		5·03					5·71
Th	19·8		16·5					14·0
Tl	0·497		0·364					0·161
U	3·53		2·46					4·03
V	71		119	*80*	*74*	*127*	*142*	192
W	0·733		2·88					0·937
Y	20·2		28·7					30·0
Zn	90·0		91·0	*84*	*101*	*117*	*79*	103
Zr	*410*		*413*	*409*	*438*	*364*	*382*	468
La	67·0		83·3					84·3
Ce	111		163					156
Pr	11·7		17·4					16·7
Nd	39·3		60·8					59·2
Sm	6·40		9·80					9·70
Eu	1·52		2·47					2·59
Gd	4·85		7·49					7·52
Tb	0·700		1·07					1·08
Dy	3·83		5·73					5·84
Ho	0·71		1·05					1·09
Er	1·87		2·65					2·86
Tm	0·274		0·373					0·416
Yb	1·76		2·30					2·70
Lu	0·251		0·315					0·392
Eu/Eu*	0·83		0·88					0·92
Isotope compositions								
$^{87}Sr/^{86}Sr$	0·705450	0·705324	0·705616	0·706171	0·704876		0·704782	0·704651
± 2σ	24	15	15	14	14		14	14
$^{87}Sr/^{86}Sr$ (20 Ma)	0·705035		0·705434	0·705962	0·704781		0·704491	0·704532
$^{143}Nd/^{144}Nd$	0·512658		0·512635	0·512518	0·512653		0·512624	0·512655
± 2σ	14		9	11	13		14	8
εNd	+0·4		-0·1	-2·3	+0·3		-0·3	+0·3
εNd (20 Ma)	+0·2		-0·2					+0·2
$^{176}Hf/^{177}Hf$	0·282857		0·282782	0·282808	0·282877		0·282877	0·282916
± 2σ	7		7	7	6		6	8
εHf	+3·0		+0·4	+1·3	+3·7		+3·7	+5·1
εHf (20 Ma)	+2·8		+0·1					+5·0

(continued)

Table 3: Continued

Sample code:	SG	SG	SG	SG	SG	SG	SG	SG
Sample no.:	6	7	11	12	18	22	23	27
Rock type:	Phonotephrite	Tephriphonolite	Basanite	Basanite	Basanite	Basanite	Basanite	Basanite
Location:	Löwenburg	Scheerkopf	Arzdorf (reassay of sample V-34)	Wachtberg (reassay of sample V-107)	Eulenberg	Asberg	Hasenhardt	Römerich
Trace elements (ppm)								
Ba	953	*895*	688	730	678	554	575	552
Co	19·0		55·8	55·7	53·2	52·1	53·4	49·4
Cr	52·0	*73*	397	350	481	336	348	205
Cs	5·09		0·923	0·609	0·652	0·557	0·371	0·400
Cu	29·1		58·0	59·0	54·2	63·4	65·7	53·3
Ga	26·3		19·2	19·4	19·2	19·6	19·9	20·3
Hf	8·74		4·79	4·79	5·00	4·88	4·93	5·17
Li	25·4		8·80	8·90	13·8	7·70	7·90	12·6
Mo	3·82		2·82	1·72	1·92	2·50	2·63	1·87
Nb	100·6	*90*	87·1	78·5	84·4	66·0	68·9	82·1
Ni	32·0	*35*	285	231	317	232	248	131
Pb	12·5		3·78	2·82	3·96	3·28	3·14	2·20
Rb	114	*120*	28·3	49·6	36·5	21·6	33·1	31·7
Sb	0·422		0·179	0·131	0·156	0·111	0·117	0·082
Sc	10·0	*13*	25·2	30·0	25·8	26·0	26·8	27·1
Sr	944	*812*	810	725	933	737	755	814
Ta	5·37		4·83	4·46	4·63	3·83	4·10	5·65
Th	16·5		7·49	6·06	7·51	5·69	5·72	4·20
Tl	0·241		0·0390	0·0510	0·0160	0·0330	0·0320	0·0340
U	5·37		1·84	1·72	1·82	1·45	1·49	1·01
V	158	*165*	236	289	246	239	247	278
W	2·61		1·58	0·919	1·30	1·07	1·11	0·599
Y	19·9		23·0	25·1	24·5	24·4	25·0	26·8
Zn	108	*99*	101	99·0	102	107	109	105
Zr	445	*434*	221	212	230	215	217	222
La	76·7		58·9	49·4	60·1	47·3	48·4	51·3
Ce	134		108	94·0	112	90·0	92·0	100
Pr	14·5		12·0	11·1	12·6	10·6	10·9	11·7
Nd	51·0		44·5	42·9	46·9	41·0	42·0	45·9
Sm	8·20		7·90	8·10	8·40	7·90	8·00	8·70
Eu	2·30		2·36	2·44	2·53	2·43	2·46	2·65
Gd	6·09		6·60	6·97	7·10	6·83	6·93	7·51
Tb	0·820		0·920	0·980	0·990	0·980	0·990	1·06
Dy	4·15		4·86	5·26	5·24	5·25	5·31	5·67
Ho	0·730		0·860	0·940	0·930	0·940	0·960	1·02
Er	1·81		2·09	2·31	2·27	2·30	2·33	2·48
Tm	0·248		0·282	0·313	0·303	0·310	0·312	0·332
Yb	1·54		1·70	1·88	1·83	1·86	1·90	1·97
Lu	0·224		0·236	0·264	0·251	0·260	0·262	0·275
Eu/Eu*	0·99		1·00	0·99	1·00	1·01	1·01	1·00
Isotope compositions								
$^{87}Sr/^{86}Sr$	0·704334	0·704330	0·703485	0·703461		0·703591	0·703600	0·703368
± 2σ	12	13	14	15		13	14	13
$^{87}Sr/^{86}Sr$ (20 Ma)	0·704235	0·704209	0·703457	0·703405		0·703567	0·703564	0·703336
$^{143}Nd/^{144}Nd$	0·512778	0·512730	0·512796	0·512827		0·512847	0·512867	0·512864
± 2σ	8	12	13	12		6	7	10
εNd	+2·7	+1·8	+3·1	+3·7		+4·1	+4·5	+4·4
εNd (20 Ma)	+2·6		+2·9	+3·5		+3·8	+4·2	+4·2
$^{176}Hf/^{177}Hf$	0·282901	0·282901	0·282963	0·282980		0·282974	0·282957	0·282977
± 2σ	5	7	7	8		7	7	6
εHf	+4·6	+4·6	+6·7	+7·4		+7·1	+6·5	+7·2
εHf (20 Ma)	+4·5		+6·7	+7·3		+7·0	+6·4	+7·1
$^{206}Pb/^{204}Pb$			19·630			19·573	19·582	19·573
± 2σ			5			4	6	7
$^{206}Pb/^{204}Pb$ (20 Ma)			19·531			19·483	19·486	19·479
$^{207}Pb/^{204}Pb$			15·646			15·636	15·634	15·634
± 2σ			5			5	7	9
$^{207}Pb/^{204}Pb$ (20 Ma)			15·642			15·632	15·629	15·629
$^{208}Pb/^{204}Pb$			39·506			39·433	39·430	39·409
± 2σ			6			5	8	11
$^{208}Pb/^{204}Pb$ (20 Ma)			39·373			39·317	39·309	39·281

(continued)

Table 3: Continued

Sample code:	SG	SG	SG	SG	SG	SG	SG	SG
Sample no.:	29	30	21	4	13	14	16	17
Rock type:	Basanite	Basanite	Basanite	Tephrite	Tephrite	Tephrite	Tephrite	Tephrite
Location:	Schwarzer See	Erpeler Ley	Groβer Weilberg (reassay of sample V-55)	Löwenburg	N Ölend (reassay of sample V-30.1)	Kuckstein, Oberkassel (reassay of sample V-74)	N Pleiserhohn	Stuxenberg (reassay of sample V-96)
Trace elements (ppm)								
Ba	*555*	644	*831*	785	*777*	801	722	*809*
Co		52·5		34·5		49·7	53·7	
Cr	*372*	259		169		354	438	*681*
Cs		0·861		1·73		4·39	3·99	
Cu		51·2		47·6		60·1	65·1	
Ga		21·5		24·9		20·4	19·2	
Hf		5·73		8·07		5·26	4·98	
Li		11·4		19·0		9·40	8·60	
Mo		2·06		7·15		2·00	2·84	
Nb	*65*	76·2	*60*	86·7	*87*	92·6	79·0	*100*
Ni	*233*	206		90		197	262	*162*
Pb		4·27		8·30		3·86	3·69	
Rb	*21*	49·1	*34*	80·4	*26*	30·8	26·3	*43*
Sb		0·159		0·266		0·161	0·145	
Sc	*35*	26·1	*27*	18·4	*11*	28·6	26·5	*17*
Sr	*722*	825	*778*	1091	*744*	794	907	*1028*
Ta		4·26		4·76		5·12	4·21	
Th		6·95		10·8		7·92	7·06	
Tl		0·0340		0·0960		0·0160	0·0500	
U		1·80		3·24		1·87	1·81	
V	*245*	261	*246*	221	*258*	247	244	*245*
W		1·02		2·87		1·23	1·16	
Y		26·2		23·5		24·9	26·0	
Zn	*102*	113	*114*	120	*96*	103	108	*141*
Zr	*228*	259	*229*	388	*240*	245	225	*258*
La		54·8	49	73·2	72	56·0	59·9	68
Ce		105	106	139	135	103	112	138
Pr		12·2	9	15·8	13	11·6	12·9	14
Nd		46·6		58·6		43·3	48·7	
Sm		8·80	6·5	10·0	7·9	7·90	8·90	8·9
Eu		2·65	2·69	2·85	2·71	2·35	2·66	2·53
Gd		7·50		7·63		6·70	7·45	
Tb		1·05	0·9	1·02	0·84	0·950	1·05	0·93
Dy		5·57	5·5	5·13	5·8	5·13	5·58	5·1
Ho		0·990	1·04	0·890	1·01	0·930	0·990	0·98
Er		2·39	2·6	2·13	2·9	2·30	2·40	2·3
Tm		0·318		0·284		0·316	0·321	
Yb		1·90	1·8	1·71	1·9	1·92	1·90	1·5
Lu		0·262	0·26	0·239	0·28	0·274	0·261	0·32
Eu/Eu*		0·99		0·99		0·98	1·00	
Isotope compositions								
$^{87}Sr/^{86}Sr$		0·703560	0·703780	0·704367	0·70368	0·703714	0·703519	0·70343
± 2σ		14	40	12		13	13	
$^{87}Sr/^{86}Sr$ (20 Ma)		0·703511	0·703744	0·704307	0·703651	0·703682	0·703496	0·703396
$^{143}Nd/^{144}Nd$		0·512844	0·512809	0·512745		0·512854	0·512820	
± 2σ		4	10	12		13	14	
εNd		+4·0	+3·3	+2·1		+4·2	+3·6	
εNd (20 Ma)		+3·8		+1·9		+4·0	+3·3	
$^{176}Hf/^{177}Hf$		0·282955		0·282857		0·282971	0·282980	
± 2σ		6		6		6	7	
εHf		+6·5		+3·0		+7·0	+7·4	
εHf (20 Ma)		+6·4		+2·9		+7·0	+7·3	
$^{206}Pb/^{204}Pb$			19·402	19·455		19·591		
± 2σ			9	3		5		
$^{206}Pb/^{204}Pb$ (20 Ma)				19·376		19·492		
$^{207}Pb/^{204}Pb$			15·655	15·656		15·656		
± 2σ			10	4		7		
$^{207}Pb/^{204}Pb$ (20 Ma)				15·652		15·651		
$^{208}Pb/^{204}Pb$			39·315	39·335		39·519		
± 2σ			32	5		8		
$^{208}Pb/^{204}Pb$ (20 Ma)				39·249		39·382		

(continued)

Table 3: Continued

Sample code:	SG	SG	SG	SG	SG	SG	SG	SG
Sample no.:	25	28	31	19	20	26	24	15
Rock type:	Tephrite	Tephrite	Alkali basalt	Alkali basalt	Alkali basalt	Alkali basalt	Hawaiite	Subalkaline basalt
Location:	Oberplag	Dattenberger Wald	Rödderhof	Petersberg (reassay of sample V-31a)	Ölberg	Strödter Hügel	Kietzhaus	Scharfenberg
Trace elements (ppm)								
Ba	760	*547*	726	793	707	763	538	417
Co	46·2		47·0	49·8	45·7	49·9	45·2	49·2
Cr	132	*73*	294	256	278	264	187	245
Cs	0·686		0·887	0·388	0·434	0·399	0·361	0·332
Cu	55·8		64·0	68·1	67·7	56·5	55·9	60·7
Ga	22·1		20·5	20·8	20·0	20·9	20·4	20·4
Hf	6·00		4·88	4·78	4·82	4·95	4·82	4·07
Li	11·1		9·80	6·20	7·40	6·30	6·30	9·50
Mo	2·69		3·13	2·10	1·70	2·04	1·33	1·37
Nb	98·7	*69*	80·5	63·2	72·5	66·2	58·1	50·9
Ni	88·0	*50*	169	182	173	185	119	155
Pb	3·55		4·01	2·72	3·19	2·95	2·48	1·99
Rb	40·3	*32*	51·5	35·1	36·8	35·8	34·5	27·3
Sb	0·141		0·166	0·0900	0·107	0·0910	0·0830	0·0790
Sc	25·3	*21*	27·9	25·4	27·3	25·6	24·7	26·8
Sr	959	*733*	827	796	786	832	657	628
Ta	5·73		4·51	3·41	4·15	3·57	3·39	3·05
Th	7·64		7·46	5·33	6·31	5·58	4·32	3·55
Tl	0·0360		0·0190	0·0260	0·0340	0·0420	0·0420	0·0280
U	1·91		1·77	1·41	1·45	1·47	1·06	0·900
V	281	*283*	253	217	237	219	230	229
W	0·818		1·59	1·11	0·941	0·988	0·685	0·581
Y	30·9		26·9	25·8	25·2	26·0	23·3	24·6
Zn	116	*99*	104	119	100	121	105	112
Zr	275	*223*	220	218	219	231	205	167
La	67·2		56·7	49·0	48·6	50·7	36·5	37·7
Ce	129		106	90·0	89·0	94·0	71·0	73·0
Pr	15·0		11·8	10·3	10·2	10·7	8·60	8·70
Nd	57·5		43·9	39·2	38·9	40·6	34·2	34·5
Sm	10·6		8·00	7·60	7·40	7·70	6·90	7·10
Eu	3·20		2·41	2·35	2·28	2·40	2·19	2·24
Gd	8·96		6·97	6·74	6·60	6·88	6·29	6·43
Tb	1·25		1·00	0·980	0·950	1·00	0·900	0·940
Dy	6·61		5·51	5·34	5·21	5·44	4·94	5·16
Ho	1·18		1·01	0·970	0·950	0·970	0·880	0·930
Er	2·84		2·54	2·39	2·37	2·38	2·15	2·26
Tm	0·378		0·352	0·319	0·325	0·321	0·287	0·305
Yb	2·22		2·16	1·92	2·00	1·91	1·76	1·80
Lu	0·311		0·305	0·265	0·281	0·264	0·245	0·247
Eu/Eu*	1·00		0·98	1·00	0·99	1·01	1·01	1·01
Isotope compositions								
$^{87}Sr/^{86}Sr$	0·703352			0·703444	0·703637	0·703521		0·703491
± 2σ	12			15	14	14		15
$^{87}Sr/^{86}Sr$ (20 Ma)	0·703317			0·703408	0·703598	0·703486		0·703456
$^{143}Nd/^{144}Nd$	0·512851			0·512862	0·512806	0·512862		0·512864
± 2σ	15			7	13	8		13
εNd	+4·2			+4·4	+3·3	+4·4		+4·4
εNd (20 Ma)	+3·9			+4·1	+3·0	+4·2		+4·1
$^{176}Hf/^{177}Hf$	0·282997			0·282986	0·282969	0·282976		0·282991
± 2σ	7			6	6	6		9
εHf	+8·0			+7·6	+7·0	+7·2		+7·7
εHf (20 Ma)	+7·9			+7·5	+6·9	+7·1		+7·6
$^{206}Pb/^{204}Pb$				19·638	19·690	19·633		
± 2σ				5	7	8		
$^{206}Pb/^{204}Pb$ (20 Ma)				19·533	19·597	19·531		
$^{207}Pb/^{204}Pb$				15·638	15·641	15·635		
± 2σ				6	9	9		
$^{207}Pb/^{204}Pb$ (20 Ma)				15·633	15·637	15·631		
$^{208}Pb/^{204}Pb$				39·482	39·623	39·464		
± 2σ				7	10	10		
$^{208}Pb/^{204}Pb$ (20 Ma)				39·351	39·490	39·337		

Data in italics were obtained by XRF.

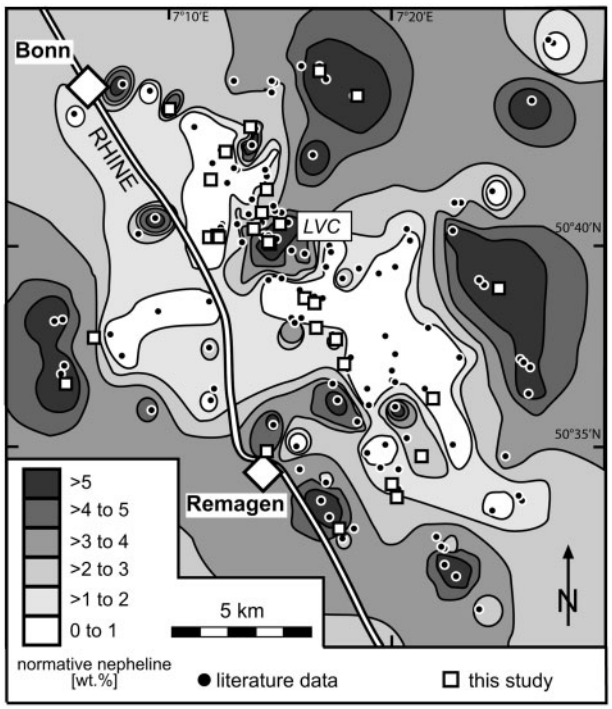

Fig. 3. Map illustrating the systematic spatial variations in SiO_2-undersaturation as expressed by the CIPW normative nepheline content. The map is based on 203 XRF analyses and contours are derived from an inverse distance squared interpolation using the Surfer software (Version 8).

observed for mafic volcanic rocks in the Vogelsberg, Hessian Depression, Rhön, and Eifel volcanic fields. Haase *et al.* (2004) defined an Eifel group (Siebengebirge, Quaternary Eifel, Hocheifel, and Westerwald; squares in Fig. 7) and a Vogelsberg group (Vogelsberg and Hessian Depression; triangles in Fig. 7) based on higher $^{87}Sr/^{86}Sr$ at a given $^{143}Nd/^{144}Nd$ in samples in the Eifel group.

In terms of Pb-isotope systematics, the compositions of the SVF mafic volcanic rocks broadly overlap with those of Westerwald lavas (Haase *et al.*, 2004); however, they are less radiogenic than mafic Tertiary rocks from the Hocheifel (Jung *et al.*, 2006). Generally speaking, samples of the Vogelsberg group have less radiogenic Pb isotopic signatures whereas Eifel group lavas comprise many samples with highly radiogenic Pb isotope ratios similar to EAR values. Compared with the other Cenozoic volcanic fields, Quaternary Eifel samples are systematically shifted to higher $^{87}Sr/^{86}Sr$ and $^{208}Pb/^{204}Pb$ values at a given $^{206}Pb/^{204}Pb$ (Wörner *et al.*, 1986).

In εHf–εNd space, the mafic SVF samples cover a narrow range completely overlapping the Rhön volcanic rocks and Vogelsberg samples analyzed by Jung *et al.* (2011), which spread over a large range in their εHf–εNd compositions (Fig. 7d).

The isotope compositions of the differentiated SVF samples are systematically more enriched than those of the mafic samples (Fig. 8). In particular, the SVF latite and trachyte samples show substantial variations in their Sr, Nd and Hf isotope compositions ($^{87}Sr/^{86}Sr = 0{\cdot}70400$–$0{\cdot}70617$; $^{143}Nd/^{144}Nd = 0{\cdot}512765$–$0{\cdot}512518$; $\varepsilon Hf = +0{\cdot}4$ to $+5{\cdot}1$). There is an increase of $^{87}Sr/^{86}Sr$ with decreasing $^{143}Nd/^{144}Nd$ (Fig. 8a) and positive co-variation in εNd–εHf space (Fig. 8b). Furthermore, an increase in $^{87}Sr/^{86}Sr$ with increasing SiO_2 concentration can be observed (Fig. 8c).

In contrast to the latite and trachyte samples, the phonotephritic to tephriphonolitic samples from the LVC show only limited variations in their Sr–Nd–Hf isotope compositions and plot at the less radiogenic end of the array defined by the felsic lavas ($^{87}Sr/^{86}Sr = 0{\cdot}704330$–$0{\cdot}704430$; $\varepsilon Nd = +1{\cdot}8$ to $+2{\cdot}7$; $\varepsilon Hf = +3{\cdot}0$ to $+4{\cdot}6$). Previously reported Sr and Nd isotope data of Wedepohl *et al.* (1994) (two analyses) are in good agreement with our data (Fig. 8a).

DISCUSSION

Origin of basanitic to alkaline basaltic melts

The limited role of fractional crystallization

The mafic volcanic rocks of the SVF have low SiO_2 (<50 wt %) and high MgO concentrations (>7 wt %), resulting in high Mg-numbers (>65) for most samples (see Table 2). The range of these Mg-numbers together with high Ni and Cr contents (mostly above 100 ppm) and the occurrence of mantle xenoliths has been used elsewhere to confirm their near-primitive nature (e.g. Frey *et al.*, 1978).

The lack of negative Eu anomalies (Fig. 6), decreasing Ni and Cr contents with decreasing MgO contents (Fig. 4b), and increasing Al_2O_3 contents with decreasing MgO (not shown) are in agreement with olivine and clinopyroxene being the predominant crystallizing phases during the early stages of fractional crystallization. The lack of significant plagioclase fractionation (lack of negative Eu anomaly) furthermore indicates that fractional crystallization probably occurred at the crust–mantle boundary at depths in excess of 15 km (Wittenbecher, 1992; Jung & Masberg, 1998; Bogaard & Wörner, 2003).

However, some of the geochemical variability observed for the mafic SVF volcanic rocks cannot be explained by fractional crystallization of cpx and olivine. For instance, at similar MgO contents the SiO_2-undersaturated basanites have higher concentrations of incompatible elements such as LREE and high field strength elements (HFSE) than the alkali basalts (Fig. 9a and b). Fractional crystallization and high degrees of crustal contamination of initially incompatible trace element enriched mafic lavas with the local basement, mainly Devonian shales, cannot

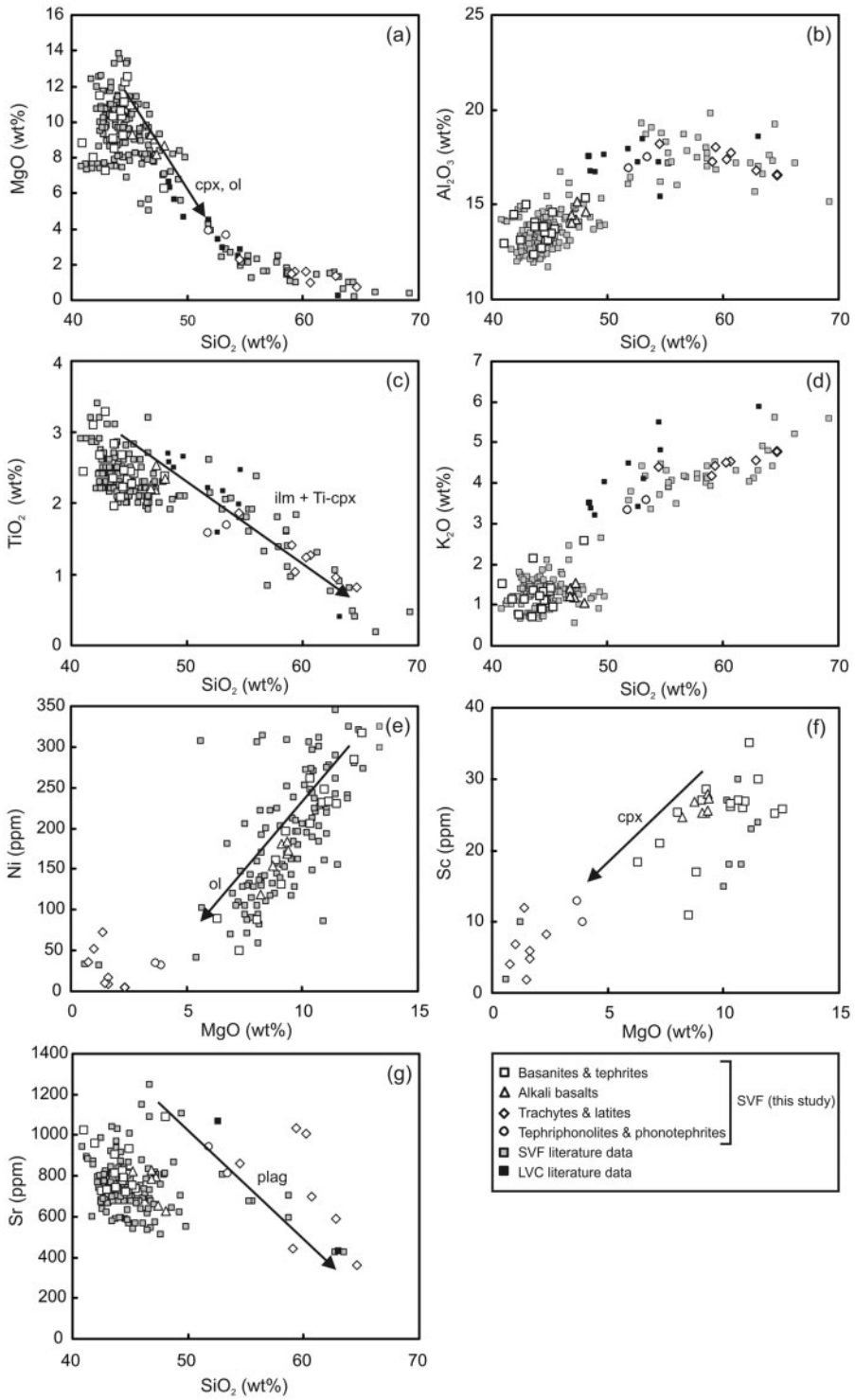

Fig. 4. Variations in the major and trace element compositions of the SVF volcanic rocks. Symbols are as in Fig. 2. (a) MgO vs SiO_2; (b) Al_2O_3 vs SiO_2; (c) TiO_2 vs SiO_2; (d) K_2O vs SiO_2; (e) Ni vs MgO; (f) Sc vs MgO; (g) Sr vs SiO_2. Black arrows indicate qualitative fractional crystallization vectors.

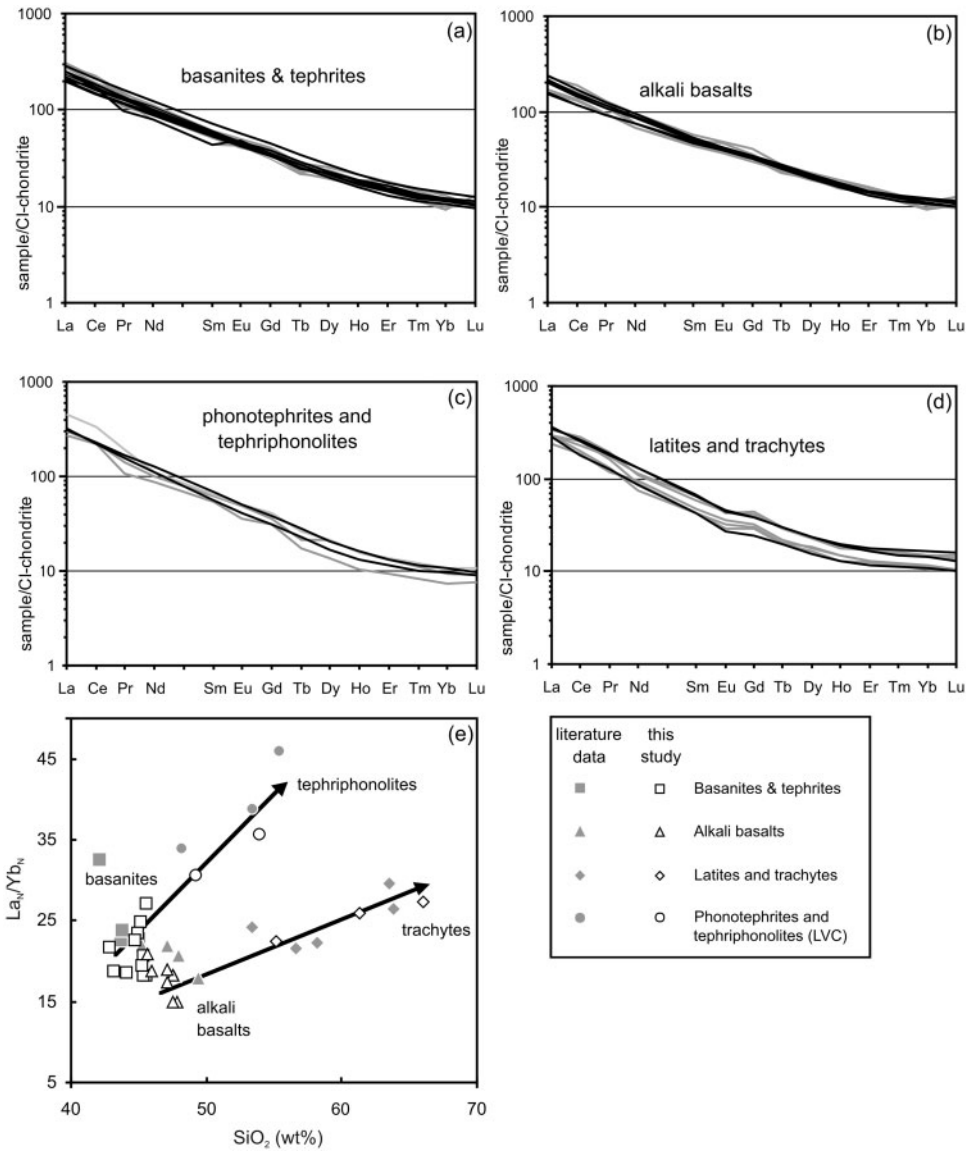

Fig. 5. CI-chondrite-normalized REE patterns of SVF volcanic rocks. (a) Basanites and tephrites; (b) alkali basalts; (c) phonotephrites and tephriphonolites (LVC); (d) latites and trachytes. Normalization values from Boynton (1984). Grey lines, literature data (Electronic Appendix); black lines, this study. (e) Variation of La_N/Yb_N vs wt % SiO_2.

explain the observed trends. Crustal contamination would additionally result in a concurrent increase of incompatible trace elements such as Rb or Ba and SiO_2. Therefore, we infer that the trace element systematics and SiO_2 variations of the mafic volcanic rocks in the SVF are primary source features. Below we explore the roles of mantle source variability, melting conditions and melting depth in controlling the primary melt compositions.

Evidence for variations in melting depth and melting degree

The composition of primary mantle melts is controlled by the mantle mineralogy, its chemical composition, degree of partial melting, and depth of melt segregation. Generally, low-degree mafic melts from the deeper upper mantle are characterized by low silica contents, high total iron contents and enrichments in incompatible trace elements such as Nb or La, compared with higher degree melts derived from shallower depths (e.g. Langmuir *et al.*, 1992).

Different degrees of melting and varying depths of melting can, for example, be tested by using ratios of incompatible elements; for example, P versus Al_2O_3. The latter is largely controlled by spinel or garnet during mantle melting, and consequently ratios of P_2O_5/Al_2O_3 are assumed to increase with increasing melting depth (Furman, 1995). The alkali basalts have distinctly lower P_2O_5/Al_2O_3 ratios

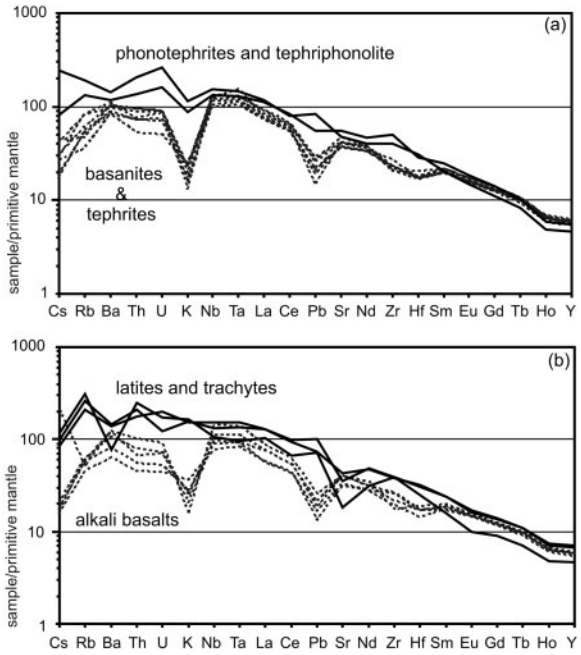

Fig. 6. Multi-element patterns normalized to the primitive mantle estimate of McDonough & Sun (1995). (a) Basanites and tephrites (dashed lines) and phonotephrites–tephriphonolites (LVC, continuous lines); (b) alkali basalts (dashed lines) and latites–trachytes (continuous lines).

(0·037–0·030) at higher SiO_2 (not shown) than the basanites and tephrites (0·062–0·038), indicating shallower melting depths for alkali basalts compared with basanites and tephrites. Strong fractionation of the HREE with $Dy_N/Yb_N > 2$ strongly indicates that the SVF lavas tap garnet-bearing mantle lithologies. The signature of residual garnet is also detectable from the high CaO/Al_2O_3 ratios in the primary melts that are controlled by residual garnet (van Westrenen *et al.*, 2001*a*; Dasgupta *et al.*, 2007).

The higher La_N/Yb_N and CaO/Al_2O_3 of the basanites and tephrites at lower SiO_2 (Figs 5e and 9d) compared with the alkali basalts are consistent with melting of garnet-bearing sources and with partial melting degrees increasing from basanitic compositions towards alkali basaltic compositions (see Herzberg, 1995; Walter, 1998; van Westrenen *et al.*, 2001*a*, 2001*b*). Hence, the negative co-variations of incompatible elements with SiO_2 (Fig. 9a–c) indicate lower degrees of melting and somewhat higher average melting depths for the strongly SiO_2-undersaturated basanites with respect to the alkali basalts.

Similar observations have been made by Haase *et al.* (2004) for the nearby Westerwald Volcanic Field (WVF), where basanitic to alkali basaltic lavas erupted at about the same time as in the SVF (20–30 Ma). Those workers estimated REE compositions (Dy_N/Yb_N and Ce_N/Yb_N) of melts derived from a modelled regional mantle source for garnet stability field and garnet–spinel transition zone conditions. Their results show that the WVF lavas could be derived by about 4–7% partial melting, mainly in the garnet stability field. In Fig. 9e, our data are compared with the Westerwald data. Overall, the SVF data exhibit somewhat similar Dy_N/Yb_N and Ce_N/Yb_N to the WVF, arguing for melting at approximately similar average depths. The SVF alkali basalts have lower Dy_N/Yb_N and Ce_N/Yb_N than the basanites and tephrites and can be explained by 5–7% partial melting within the garnet–spinel transition zone (Fig. 9e). The compositions of the basanites indicate a stronger influence of garnet-bearing peridotite at lower degrees of partial melting (3–5%) if the most mafic basanite samples are considered (MgO > 11 wt %). These samples have the highest Ce/Yb(N) ratios and also tend to higher Dy/Yb(N) than the alkali basalts. Because the transition from garnet to spinel lherzolite occurs at 2·4–2·7 GPa for typical peridotite compositions (Green & Ringwood, 1967; Robinson & Wood, 1998) it can be inferred that the Siebengebirge magmas formed at around, or just below, 70–80 km depth at about 1250–1300°C (Haase *et al.*, 2004; Jung *et al.*, 2006).

In summary, the major and trace element data indicate that the basanitic magmas are low-degree partial melts, which formed at deeper average melting depths over a shorter melting column than the alkali basalts. The alkali basalts represent higher degrees of partial melting at shallower average depths with less influence of residual garnet. Clearly, the compositions of the SVF primary magmas represent a continuous spectrum, thus indicating gradual variations of melting conditions in space and time.

Trace element evidence for eclogitic components in the asthenospheric mantle source and the influence of metasomatized lithospheric mantle

The basanites and alkali basalts of the SVF display tightly constrained compositional ranges in terms of their Sr, Hf, Nd, and Pb isotopic compositions (Fig. 7). Hence, the entire spectrum of primary mafic magmas was derived from a mantle source with fairly uniform isotope characteristics that shares similarities with the EAR or other similar mantle source components [e.g. Common Mantle Reservoir (CMR), Lustrino & Wilson, 2007; Low Velocity Component (LVC), Hoernle *et al.*, 1995; Prevalent Mantle, Wörner *et al.*, 1986; Focus Zone (FoZo); Hart *et al.*, 1992]. It has been suggested previously that the modification of the Central European mantle may be a consequence of subduction recycling during the Variscan orogeny (Wilson & Downes, 1991). Geochemical and experimental studies on the petrogenesis of oceanic island basalts (OIB) suggest the presence of recycled oceanic crust in the sources of some alkaline OIB magmas (e.g. Hofmann, 1997; Hirschmann *et al.*, 2003; Kogiso *et al.*, 2003). Clearly, melts directly derived from subducted oceanic crust (eclogite) cannot produce the highly silica-undersaturated rocks

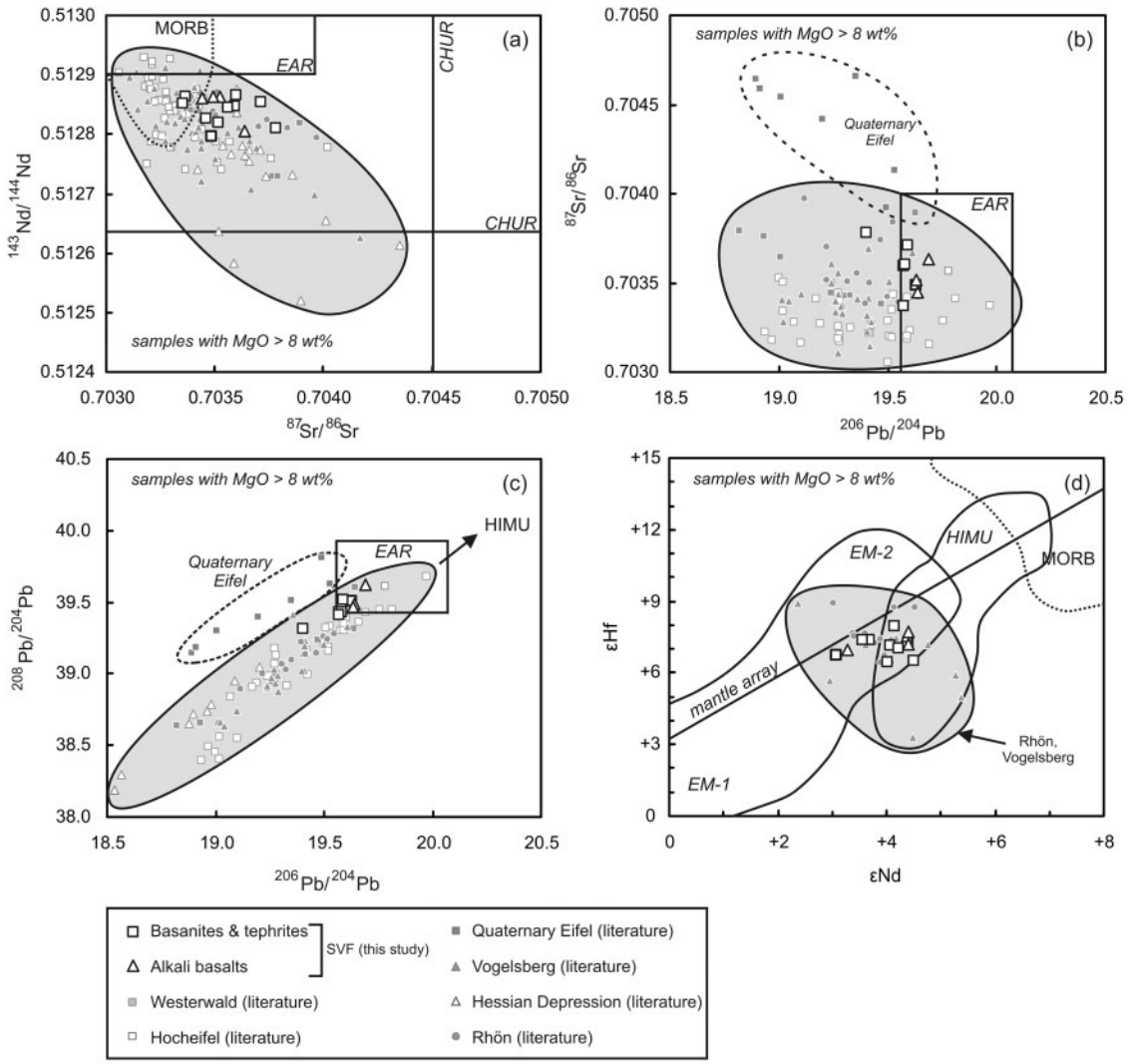

Fig. 7. Isotope geochemistry of mafic volcanic rocks with MgO >8 wt % from the SVF [data from this study, and Wörner *et al.* (1986), Vieten *et al.* (1988), Wedepohl *et al.* (1994) and Wedepohl & Baumann (1999); compiled in the Electronic Appendix] and adjacent volcanic fields in the German part of the CEVP using the compiled dataset of Lustrino & Wilson (2007) available at http://georoc.mpch-mainz.gwdg.de/georoc/website/Expert_Datasets.htm. Hafnium isotope compositions of Rhön and Vogelsberg volcanic rocks are from Jung *et al.* (2005, 2011). Mantle end-members and MORB fields (dashed lines) are from Cebriá & Wilson (1995), Hofmann (2003) and Stracke *et al.* (2005). Mantle array in εHf–εNd space is after Vervoort *et al.* (1999). (a) $^{143}Nd/^{144}Nd$ vs $^{87}Sr/^{86}Sr$; (b) $^{87}Sr/^{86}Sr$ vs $^{206}Pb/^{204}Pb$; (c) $^{208}Pb/^{204}Pb$ vs $^{206}Pb/^{204}Pb$; (d) εHf vs εNd.

found in intraplate settings, as any partial melt of a basaltic protolith would be silica-saturated (e.g. Kogiso *et al.*, 2003; Pertermann & Hirschmann, 2003). It has, therefore, previously been suggested that silica-saturated recycled oceanic crust is transformed into silica-deficient garnet-pyroxenite by melt extraction, which, during a later melting event, is capable of producing ne-normative melts similar in composition to alkaline intraplate basalts (Hirschmann *et al.*, 2003; Kogiso *et al.*, 2003). Several major and trace element characteristic of alkali basaltic lavas, however, cannot be explained by this model and the involvement of lithospheric sources has been proposed (e.g. Pilet *et al.*, 2008), which we will discuss in detail below.

The interpretation that eclogitic domains that were affected by previous melt extraction (i.e. slab melting) may be present in the local SVF mantle source is supported by the observation that the mafic SVF lavas have elevated Zr/Hf ratios (41–47; Fig. 9f). This is unusual, as many mafic rocks typically scatter around the chondritic value of $34{\cdot}2 \pm 0{\cdot}3$ (Münker *et al.*, 2003). High Zr/Hf ratios reaching values up to 45 have been observed in OIB (Pfänder *et al.*, 2007) and in continental intraplate basalts from the Eifel, Vogelsberg, and Rhön (Pfänder *et al.*, 2012). This feature has been explained by a number of petrogenetic models including clinopyroxene fractionation (David *et al.*, 2000), carbonatite metasomatism (Dupuy *et al.*,

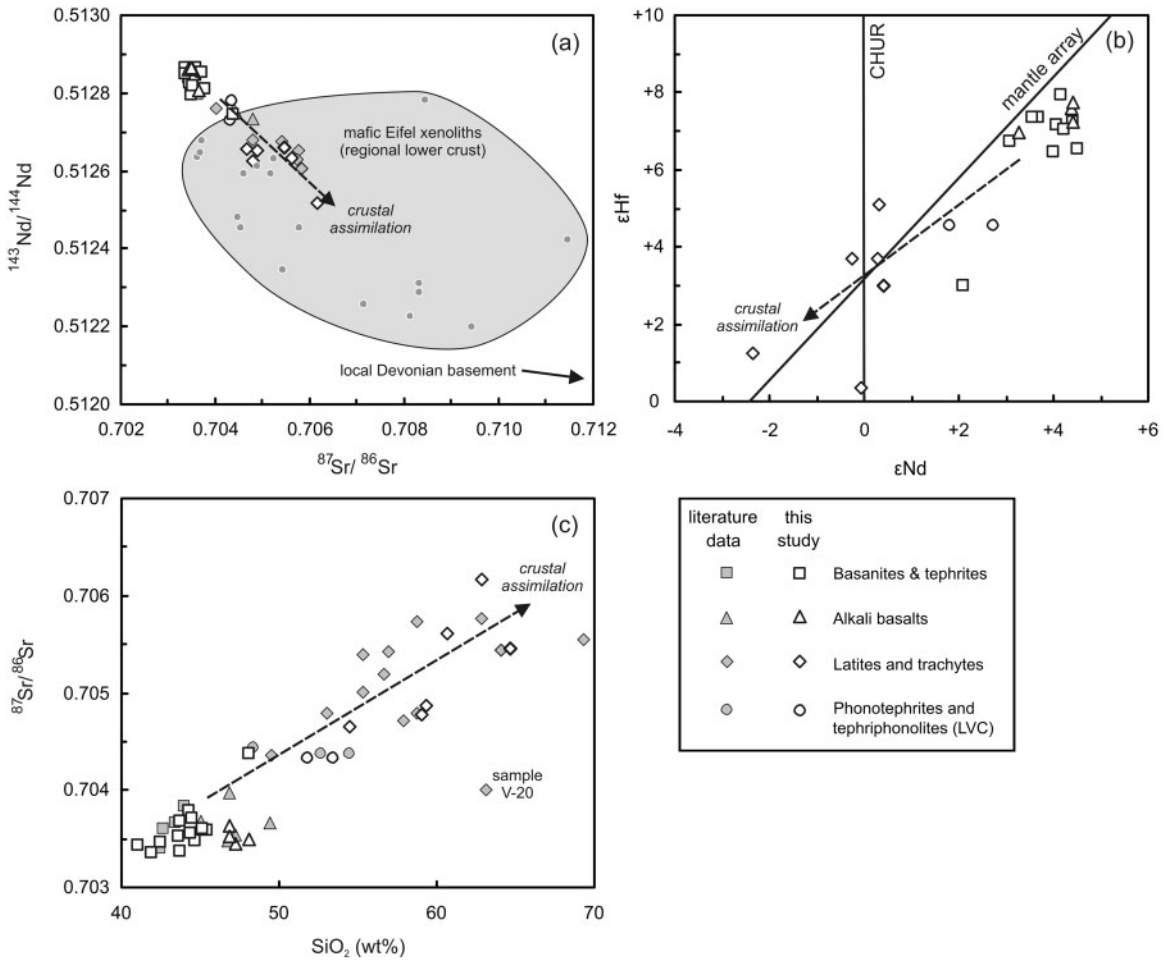

Fig. 8. Nd–Sr–Hf isotope systematics of differentiated SVF volcanic rocks compared with mafic SVF rocks. The data are from this study (Tables 2 and 3) and the published literature (Wörner *et al.*, 1986; Vieten *et al.*, 1988; Wedepohl *et al.*, 1994; compiled in the Electronic Appendix). Mafic Eifel xenoliths (metatonalites and granulites) are from Stosch & Lugmair (1984), Loock *et al.* (1990) and Stosch *et al.* (1991). (a) $^{143}Nd/^{144}Nd$ vs $^{87}Sr/^{86}Sr$. Composition of the regional Devonian basement ($^{87}Sr/^{86}Sr$ 0·74500; $^{143}Nd/^{144}Nd$ 0·511982) is from Wörner *et al.* (1982, 1985). (b) εHf vs εNd; mantle array after Vervoort *et al.* (1999) (c) $^{87}Sr/^{86}Sr$ vs SiO_2. Arrows indicate qualitatively expected vectors for assimilation of crustal material.

1992), and/or melting involving an eclogitic component (Klemme *et al.*, 2002; Pfänder *et al.*, 2007). Fractionation of clinopyroxene is not a likely process to generate the high Zr/Hf values observed, as most of the mafic magmas discussed here have near-primitive compositions and uniformly high Sc concentrations (20–35 ppm; Fig. 4c). A more important influence of carbonatitic components in the sources of the CEVP magmas (Eifel, Vogelsberg, and Rhön) has previously been proposed on the basis of high-precision HFSE measurements (Pfänder *et al.*, 2012). However, carbonatite metasomatism cannot fully explain the high Zr/Hf, as average carbonatites display similar ranges of Zr/Hf to intraplate basalts (Bizimis *et al.*, 2003; Pfänder *et al.*, 2012). Hence, the involvement of an eclogitic component seems to be a highly plausible scenario.

Melting of subducted oceanic crust in the eclogite stability field can lead to significant Zr/Hf fractionation because Hf is less compatible than Zr in the Ca-rich almandine garnet typical of eclogites (e.g. van Westrenen *et al.*, 2001*a*, *b*; Klemme *et al.*, 2002). In contrast, Zr and Hf display similar partition coefficients for pyrope garnet, which is characteristic for common mantle peridotite (e.g. Green *et al.*, 2000; van Westrenen *et al.*, 2001*a*, *b*; Klemme *et al.*, 2002). Hence, extraction of slab melts during subduction may generate residual eclogite with high Zr/Hf. Such eclogitic components (i.e. recycled oceanic crust) may be convectively incorporated into mantle peridotite and impart their high Zr/Hf characteristics to any primary mantle melts generated at a later stage (Pfänder *et al.*, 2007). The interpretation that such a scenario is relevant to the SVF lavas is corroborated by the observation that samples with the most elevated Zr/Hf display the highest La/Yb (Fig. 9f) and Nb/Y (not shown). Thus, samples with the strongest evidence for the involvement of residual garnet

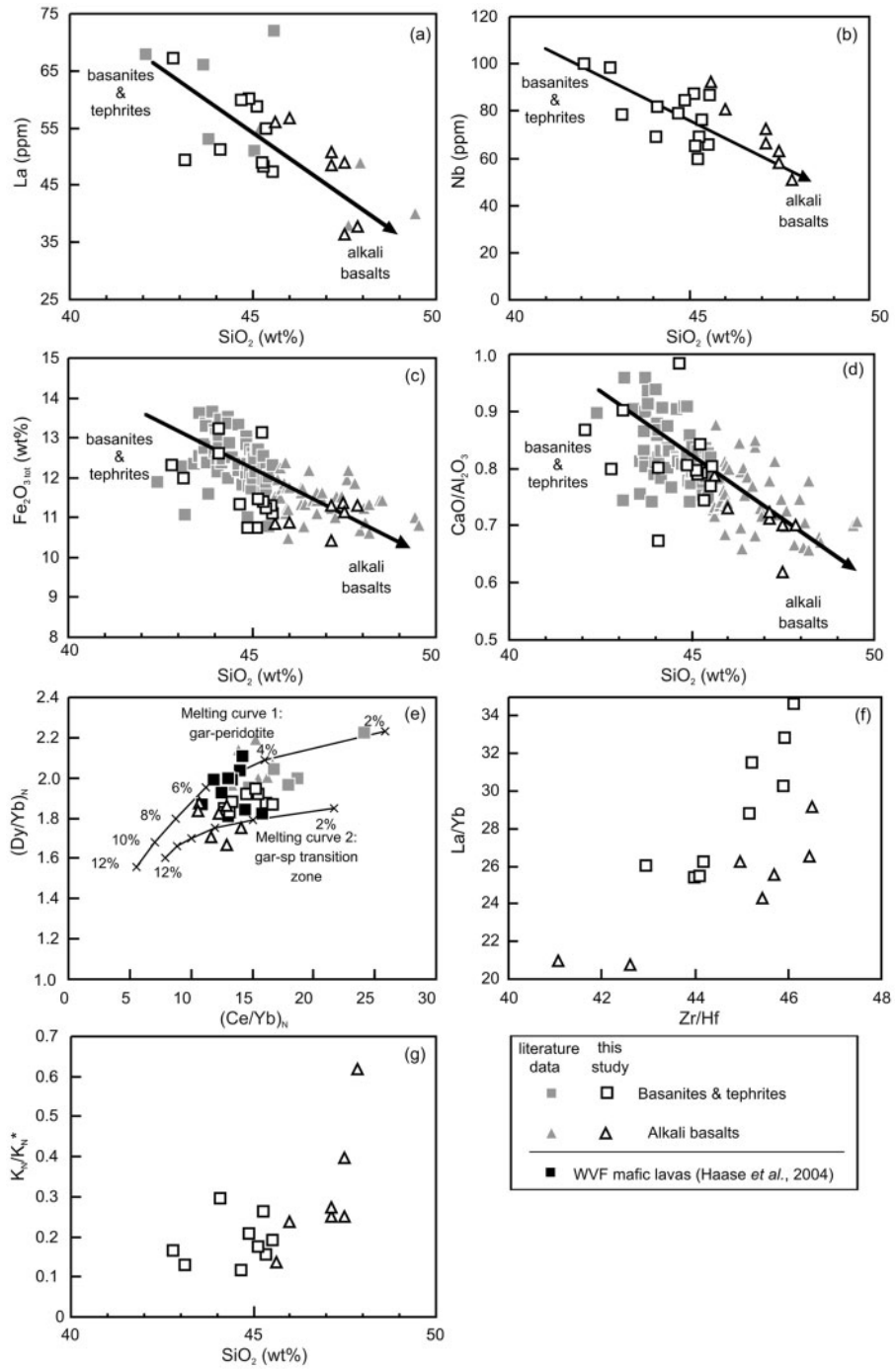

Fig. 9. Compositional variations of mafic SVF samples (<50 wt % SiO_2). (a) La, (b) Nb, (c) $Fe_2O_{3\ tot}$ and (d) CaO/Al_2O_3 vs SiO_2 wt %. (e) Variation of $(Dy/Yb)_N$ vs $(Ce/Yb)_N$. The comparison of the REE systematics of mafic SVF lavas with data from the adjacent Westerwald Volcanic Field (WVF; black squares) illustrates that the SVF primary magmas were derived by melting within and/or just below the garnet–spinel transition zone. Modelled melting curves are from Haase *et al.* (2004). Melting curve 1: modelled REE systematics of peridotite melting in the garnet stability field (55% olivine, 20% orthopyroxene, 21% clinopyroxene, 4% garnet). Data from the WVF mainly follow this trend, indicating a deep asthenospheric origin. Melting curve 2: modelled REE systematics of peridotite melting in the garnet–spinel transition zone (55% olivine, 20% orthopyroxene, 21% clinopyroxene, 1·5% garnet, 2·5% spinel). A detailed description of the REE modelling has been given by Haase *et al.* (2004). Compositions of the SVF mafic magmas point to a similar origin to the WVF primary magmas (garnet–spinel transition zone). Tick marks with numbers indicate percentages of the degree of melting. (f) La/Yb vs Zr/Hf. (g) Variation of K_N/K_N^* $[K^* = \sqrt{(U_N \times Nb_N)}]$ vs SiO_2 (wt %) for primary melts indicates the involvement of lithospheric mantle containing a K-bearing phase (phlogopite or amphibole). A decrease of the negative K anomaly with increasing melting degree (as reflected by higher SiO_2 contents) suggests a decreasing influence of lithospheric mantle components.

also display the strongest evidence for recycled eclogitic components. It is furthermore important to consider that domains of recycled eclogite within the asthenospheric mantle could lower the melting temperature (e.g. Hall & Spakman, 2002) so that a mantle plume would not necessarily be required to explain the formation of the SVF magmas (e.g. Foley, 1992; Kogiso & Hirschmann, 2001).

Another prominent compositional feature of the mafic SVF lavas is their negative K anomalies in primitive mantle normalized trace element patterns (Fig. 6), which indicate the presence of a buffering residual K-rich mineral phase, such as phlogopite or amphibole during partial melting (Class & Goldstein, 1997; Le Roex *et al.*, 2001; Späth *et al.*, 2001; Grégoire *et al.*, 2002). This is an indication for the involvement of a lithospheric mantle component, as amphibole and/or phlogopite would be unstable in a thermally anomalous mantle plume (Wallace & Green, 1991; Class & Goldstein, 1997). In support of this view, previous studies of mantle xenoliths confirm the presence of metasomatized peridotite below major portions of the CEVP (e.g. Stosch & Seck, 1980; Kramm & Wedepohl, 1990; Witt-Eickschen *et al.*, 1998). Fluid percolation in the shallow lithospheric mantle during subduction linked to the Variscan orogeny most probably caused the widespread enrichment of large ion lithophile elements (LILE) over HFSE and precipitation of amphibole in the shallow lithospheric mantle (Wörner *et al.*, 1986; Rosenbaum & Wilson, 1996; Witt-Eickschen *et al.*, 2003). Notably, the trend of increasing K_N/K_N^* $[=K_N/\sqrt{(U_N)\times(Nb_N)}]$ with SiO_2 indicates that the anomaly becomes successively less pronounced at higher average depths of partial melting (Fig. 9g). This shows that the influence of amphibole or phlogopite during melt generation decreases successively, as mantle domains rich in volatile-bearing mineral phases are preferentially tapped during the early stages of partial melting.

In summary, the overall composition of the SVF magma sources can be regarded as isotopically relatively homogeneous, largely tapping typical European asthenospheric mantle peridotite that has incorporated eclogitic domains representing recycled oceanic crust. There is also evidence for lithospheric components, as all mafic SVF samples exhibit negative K anomalies. However, despite significant variations in K_N/K_N^*, the isotopic characteristics indicating EAR-like sources remain virtually unaffected. Therefore, it can be inferred that asthenospheric magma sources were predominant. We envisage that melting columns are rooted in an asthenospheric source with EAR characteristics whereas the top portion of the melting column is located within metasomatized lithospheric mantle that imparts the negative K anomaly on the SVF primary melts. The uniform isotopic signature reflects the asthenospheric mantle source whereas variations in average melting depth and melting degree are reflected in trace element variations.

Comparison of SVF magmas with other Cenozoic volcanic centres in central Europe

Mafic lavas from the German portion of the CEVP show large compositional variations implying variable and complex petrogenetic processes. Tholeiitic basalts (e.g. Vogelsberg and Hessian Depression) indicate comparatively higher degrees of partial melting at shallower average melting depths (Wedepohl, 2000; Bogaard & Wörner, 2003) whereas strongly SiO_2-undersaturated melts such as melilitites (e.g. Urach–Hegau, Dunworth & Wilson, 1998) are derived from deeper sources (~90 km; Wilson *et al.*, 1995) at low degrees of partial melting. The volumetrically dominant basanites and alkali basalts originate from average melting depths that are bracketed by those of these end-members (~70 km; Bogaard & Wörner, 2003; Wilson & Downes, 2006). It has also been proposed recently that many tholeiites are the products of extensive crustal assimilation and thus may not represent primary magmas (Jung *et al.*, 2011).

By using elevated LREE/HREE ratios as an indicator for the presence of garnet in the mantle source it has been inferred that melting depths for the CEVP magmas range from the garnet stability field (Westerwald, Haase *et al.*, 2004; Urach–Hegau, Dunworth & Wilson, 1998; Eifel, Jung *et al.*, 2006; Rhön, Jung *et al.*, 2005) to the garnet–spinel transition zone (~70 km; Vogelsberg, Bogaard & Wörner, 2003; Hessian Depression, Kramm & Wedepohl, 1990; Siebengebirge, Vieten *et al.*, 1988). However, the common negative K anomalies in primitive mantle-normalized multi-element plots also indicate the influence of lithospheric mantle sources. Interestingly, negative K anomalies are absent in tholeiitic basalts, which is consistent with the interpretation that the K-bearing phase is completely consumed under these high degrees of partial melting (Wilson & Downes, 2006).

Based on Sr–Nd–Pb isotope systematics, it may be inferred that the CEVP mantle sources are characterized by mixing of a common asthenospheric component (EAR) with different regional mantle components. Overall, the isotopic characteristics of the mafic rocks in the SVF are similar to the compositions from the adjacent Paleogene volcanic fields, namely the Hocheifel and Westerwald (Haase *et al.*, 2004; Jung *et al.*, 2006; Fekiacova *et al.*, 2007*a*, 2007*b*). The Pb isotope compositions of Westerwald and Siebengebirge lavas completely overlap whereas Hocheifel lavas display the most radiogenic Pb isotope compositions. The large variability in Pb isotope composition observed in the CEVP basalts (Fig. 7c) might be explained by a variable component of recycled oceanic crust in their sources.

In contrast to the Paleogene and Neogene volcanic fields, the Quaternary Eifel volcanic field taps a mantle source with distinctive isotopic characteristics (high $^{87}Sr/^{86}Sr$, low $^{143}Nd/^{144}Nd$, low $^{206}Pb/^{204}Pb$, high

$^{208}Pb/^{204}Pb$; Fig. 7) that was apparently unavailable for partial melting during Paleogene and Neogene times. This finding is corroborated by the results of seismic tomography, identifying a plume-like mantle domain beneath the Eifel for which elevated temperatures have been proposed (Ritter *et al.*, 2001). The present-day Eifel plume may tap deeper asthenospheric mantle with a distinctive history, thereby providing a new source for magma generation ~14 Myr after the Paleogene to Neogene volcanism in the region had become extinct.

Origin of the differentiated magmas

Fractional crystallization and crustal assimilation

Major and trace element data (Fig. 4) as well as petrographic observations suggest that the petrogenesis of the latites and trachytes involved the fractionation of olivine, clinopyroxene, amphibole, plagioclase, apatite, and ilmenite from alkali basaltic primary magmas. The phonotephrites and tephriphonolites of the LVC group evolved from basanitic primary melts, and plagioclase was absent during their differentiation. The two differentiation trends are illustrated by two distinctive trends in a plot of SiO_2 versus La_N/Yb_N (Fig. 5e). The high La_N/Yb_N trend defined by the basanite to tephriphonolite samples reflects the prominent role of clinopyroxene fractionation causing progressive LREE enrichment in the melt. Magmatic differentiation defined by the alkali basalt to trachyte samples is characterized by a minor increase of La_N/Yb_N. This could be related to the lower initial LREE/HREE ratios in the primary melts (e.g. to slightly higher degrees of melting), lower amounts of clinopyroxene fractionated, and the onset of plagioclase fractionation with high D_{LREE}/D_{HREE} (e.g. Blundy *et al.*, 1998) counterbalancing the effect of clinopyroxene fractionation.

With increasing SiO_2 the differentiated samples display increasing $^{87}Sr/^{86}Sr$ and decreasing εNd and εHf values (Fig. 8). This indicates open-system behavior during differentiation associated with crustal contamination. This can be illustrated based on the Drachenfels trachyte SG 1, which contains large sanidine megacrysts (see the Electronic Appendix). The $^{87}Sr/^{86}Sr$ of the sanidine megacryst separate is lower than the $^{87}Sr/^{86}Sr$ of the whole-rock sample (sanidine 0·70532; bulk-rock 0·70545; Table 3). This observation indicates that crustal assimilation into the remaining melt phase of the Drachenfels magma continued even after crystallization of the sanidine megacrysts. Furthermore, the trend defined by the differentiated samples in $^{87}Sr/^{86}Sr$–εNd space (Fig. 8a) indicates that regional lower crust, represented by Eifel granulite xenoliths, might be considered as a potential contaminant (Stosch & Lugmair, 1984; Loock *et al.*, 1990; Rudnick & Goldstein, 1990; Stosch *et al.*, 1991). However, it cannot be ruled out that the assimilation of upper crustal materials (i.e. Devonian shales) might also have occurred to a certain degree. The upper crustal rocks have more enriched isotopic signatures ($^{87}Sr/^{86}Sr = 0{\cdot}74500$; $\varepsilon Nd = -12{\cdot}8$; Wörner *et al.*, 1982, 1985) and have previously been shown to have been involved in the petrogenesis of the Laacher See Volcano (13 ka; East Eifel Volcanic Field) (Wörner *et al.*, 1985). It is, however, debatable if the thermal conditions of the mid- to upper crust are sufficient to melt such shales and incorporate them into the differentiated melts.

The SVF magmas locally also evolved to differentiated compositions without significant interaction with crustal rocks. This is shown by trachyte sample V-20 of Wedepohl *et al.* (1994), which displays a considerably less radiogenic Sr isotope composition ($^{87}Sr/^{86}Sr = 0{\cdot}70400$) and more radiogenic Nd isotope composition ($^{143}Nd/^{144}Nd = 0{\cdot}512765$) than SVF samples with similar SiO_2 contents (see also Fig. 8c). This trachyte sample might have retained its original Sr–Nd isotope composition during the course of more or less closed-system fractional crystallization.

EC-AFC modelling

To quantify the effects of crustal assimilation during differentiation of the SVF magmas, energy-constrained AFC modelling (EC-AFC) was performed (Bohrson & Spera, 2001; Spera & Bohrson, 2001). The results of the modelling are illustrated in Fig. 10 and the modelling parameters used are summarized in Table 4. As starting composition we chose the most primitive alkali basalt sample (SG 20), which has a high MgO content (9·3 wt %), high Cr and Ni abundances and unradiogenic Sr and radiogenic Nd isotope compositions (see Tables 2 and 3). We modelled an EC-AFC process for three possible lower to mid-crustal assimilants, as follows.

(1) Granulite sample S6 from the dataset provided by Loock *et al.* (1990) was chosen as it represents the end-member of the Eifel granulite xenolith suite with the highest $^{87}Sr/^{86}Sr$ and lowest $^{143}Nd/^{144}Nd$. The concentrations of Sr (278 ppm) and Nd (20·2 ppm) are at the lower end of the mafic granulite xenolith suite (see literature data in Fig. 10).

(2) Granulite sample S32 of Stosch & Lugmair (1984) is characterized by a less radiogenic Sr and a more radiogenic Nd isotope composition (see Table 4). However, in contrast to sample S6, S32 exhibits high Sr (1325 ppm) and Nd concentrations (25·0 ppm). This sample was also previously used as assimilant in the EC-AFC models of Bogaard & Wörner (2003) and Jung *et al.* (2006).

(3) A Devonian slate from Wörner *et al.* (1982, 1985) was taken to model assimilation of metapelitic material at mid-crustal levels. Compared with the granulite samples, the slate sample is highly radiogenic in Sr and unradiogenic in Nd, and it is characterized by lower

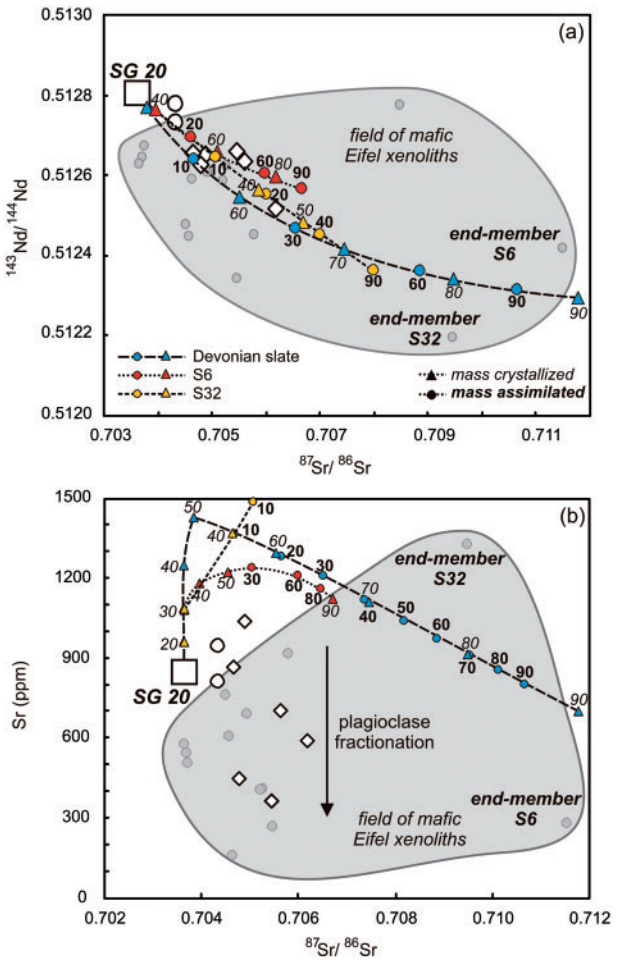

Fig. 10. EC-AFC model for the differentiated Siebengebirge samples after Spera & Bohrson (2001). End-members used for the calculation comprise representative granulitic and metapelitic compositions and are given in Table 4. (a) $^{143}Nd/^{144}Nd$ vs $^{87}Sr/^{86}Sr$; (b) $^{87}Sr/^{86}Sr$ vs Sr (ppm). Grey circles denote mafic Eifel xenoliths (granulites and metatonalites) from Stosch & Lugmair (1984), Loock *et al.* (1990) and Stosch *et al.* (1991).

Table 4: Parameters used for EC-AFC modelling [following Bohrson & Spera (2001) and Spera & Bohrson, 2001)]

	Granulites	Devonian slate
Thermal parameters		
Magma liquidus temperature	1320°C	1320°C
Magma initial temperature	1320°C	1320°C
Assimilant liquidus temperature	1100°C	700°C
Assimilant initial temperature	900°C	400°C
Solidus temperature	950°C	600°C
Equilibration temperature	980°C	650°C
Crystallization enthalpy	396000 J kg^{-1}	396000 J kg^{-1}
Isobaric specific heat of magma	1484 J kg^{-1}	1484 J kg^{-1}
Fusion enthalpy	354000 J kg^{-1}	354000 J kg^{-1}
Isobaric specific heat of assimilant	1388 J kg^{-1}	1388 J kg^{-1}
Compositional parameters		
	Sr (ppm)	Nd (ppm)
Magma SG 20	786	38·9
Bulk distribution coefficient	0·1	0·1
Enthalpy	0	0
Assimilant S6	278	20·2
Assimilant S32	1325	36·9
Devonian slate	98	25
Bulk distribution coefficient	0·5	0·25
Enthalpy	0	0
	$^{87}Sr/^{86}Sr$	$^{143}Nd/^{144}Nd$
Magma SG 20	0·703637	0·512806
Assimilant S6	0·71153	0·51242
Assimilant S32	0·70948	0·512198
Devonian slate	0·745	0·511981

Sr and Nd concentrations than the granulite samples (Table 4).

It is apparent from Fig. 10a that granulite sample S6 as assimilant can reproduce the ranges of Sr–Nd isotope compositions of the differentiated SVF lavas. However, although for the phonotephrites and tephriphonolites the amount of assimilated material (~15%) and fractional crystallization required (~50%) might still be realistic, the Sr–Nd isotope composition of the latites and trachytes require unrealistically high amounts of assimilated material (~30–90%). For the metapelite sample as well as for the granulite sample S32, however, only up to *c.* 30 % of assimilated material is required to explain the most radiogenic isotope composition of the differentiated SVF lavas.

The modelling results show that for a more detailed approach, a much better characterization of the lower crust beneath the SVF is clearly required. In particular, the end with the most radiogenic Sr isotope compositions is hitherto defined by only three samples.

A feature that also cannot be fully explained by EC-AFC modelling is the elemental Sr budget of the differentiated SVF lavas. The Sr concentrations of the differentiated SVF samples are much lower than modelled, indicating a much larger volume of fractionated plagioclase than predicted by the EC-AFC model. This assumption is supported by the negative correlation of SiO_2 with Sr concentrations in the SVF samples (Fig. 4e). However, a pronounced negative Eu anomaly is present only in the trachyte samples SG 1 and SG 2 (only ~0·8), and is lacking in other differentiated samples for which trace element data are available. As established in the studies of Weill &

Drake (1973) and Drake (1975) the ratio of Eu^{2+} to Eu^{3+} between plagioclase and the respective magmatic liquid is largely dependent on temperature and oxygen fugacity. Hence, the lack of an Eu anomaly in some of the differentiated SVF lavas might simply be attributed to T and elevated fO_2 conditions in favour of Eu^{3+}, which preferentially partitions into the melt rather than into plagioclase.

In summary, EC-AFC modelling shows that only some lower crustal compositions found in Eifel granulite xenoliths are suitable assimilants for the differentiated SVF lavas; metapelitic compositions also constitute a potential end-member. However, a more comprehensive dataset for the basement rocks beneath the SVF is clearly required to place tighter constraints on possible AFC scenarios. The EC-AFC model also fails to reproduce the low Sr concentrations in the differentiated SVF lavas. This could reflect two issues: first, the Sr concentration in the parental basaltic liquid might have been significantly lower than actually observed in the alkali basalts sampled; second, plagioclase fractionation may have been surpressed in deep crustal magma chambers, leading to increased plagioclase fractionation at shallower crustal levels.

PETROGENETIC MODEL

Generation of SVF magmas triggered by passive upwelling of enriched asthenospheric mantle

As demonstrated in Fig. 3 the SVF lavas show strong spatial gradients in their degree of SiO_2-undersaturation, expressed as abundances of normative nepheline. Among the mafic lavas, the alkali basalts occur in a broad NW–SE-trending inner zone of the SVF. In contrast, more undersaturated basanites are concentrated along the outer portions of the SVF. However, there are also some occurrences in the inner zone including the prominent LVC. To accommodate these observations, we propose a petrogenetic model that closely links SVF magmatism with lithospheric thinning beneath the Cologne Embayment (Fig. 11).

Considering the different melting depths and variation in melting degree inferred above, we argue that the observed spatial trends in the compositions of the mafic magmas reflect continuous thinning of the lithosphere. This inferred link between tectonic extension and magmatism is also consistent with the observed age patterns. Rifting of the Cologne Embayment started in the middle Oligocene at *c.* 28 Ma (Ziegler, 1992), virtually contemporaneously with initial SVF magmatism, and therefore could be the cause for the major phase of SVF volcanism, which took place between 27 and 24 Ma (including 16 of the 22 sites dated; Fig. 1c). Based on the lower melting degrees and greater average melting depths, it seems likely that the SVF basanites were the first magmas to erupt (Fig. 11a). This interpretation is corroborated by recent dating results (Linthout *et al.*, 2009), which show that strongly SiO_2-undersaturated primary melts (i.e. high normative nepheline contents) were emplaced during the early stage of SVF activity (30–24 Ma; $n = 5$; Fig. 12).

As a result of continued lithospheric thinning, and associated upwelling of the asthenosphere, alkali basaltic melts were generated at higher melting degrees and shallower average melting depths (Fig. 11b). The range of ages available for alkali basalts from the SVF (25–19 Ma; $n = 7$; Fig. 12) supports this conclusion. In this regard it is important to note that mafic SVF volcanic rocks represent a continuous compositional spectrum, which is consistent with a gradual progression of lithospheric thinning. The eruption of the alkali basalts and their differentiated products appears to be concentrated in the zone of most intense upwelling beneath the central portion of the SVF. Magmatism ceased when the peak of the rifting episode had passed and enriched mantle domains were possibly exhausted.

We would like to caution that the temporal shift from strongly SiO_2-undersaturated basanitic melts to alkali basalts claimed here relies on age information that was mostly generated by K–Ar dating in the 1980s (Fig. 1c). Clearly, additional dating by Ar–Ar methods is required to further substantiate our conclusions. However, the most recent age determinations by Ar–Ar techniques (Linthout *et al.*, 2009) have identified basanitic samples as the products of the earliest volcanic activity in the SVF ($27{\cdot}4 \pm 0{\cdot}6$ Ma, Godesburg, locality R in Fig. 1; $29{\cdot}9 \pm 0{\cdot}6$ Ma, Erpler Ley, locality Q in Fig. 1). Interestingly, the trachytes and latites of the central SVF, which have been extensively dated by Todt & Lippolt (1980), yield consistent ages between 26 and 25 Ma (Fig. 1). This feature is intriguing because the oldest alkali basalt sample, representing the potential parental melt to the latites and trachytes, dated so far is still about ~1 Myr younger (Todt & Lippolt, 1980). If this age relationship could be confirmed it would indicate that the moderately SiO_2-undersaturated magmatism started with felsic eruptions.

Causes for Central European intraplate volcanism and implications for the SVF

Cenozoic volcanism in Central Europe is spatially and temporally linked to intracontinental rifting and basement uplift, which, in turn, is a consequence of the Africa–Eurasia collision (Wilson & Downes, 1991; Wilson & Patterson, 2001). A connection to hotspot-related volcanism and lower mantle sources has been inferred on the basis of Sr–Nd–Pb isotopic similarities to OIB lavas (e.g. Wedepohl & Baumann, 1999), relying on the assumption that oceanic island basalts are derived from a deep mantle source. Other geochemical and geophysical models for the CEVP have traditionally involved mantle plumes (e.g.

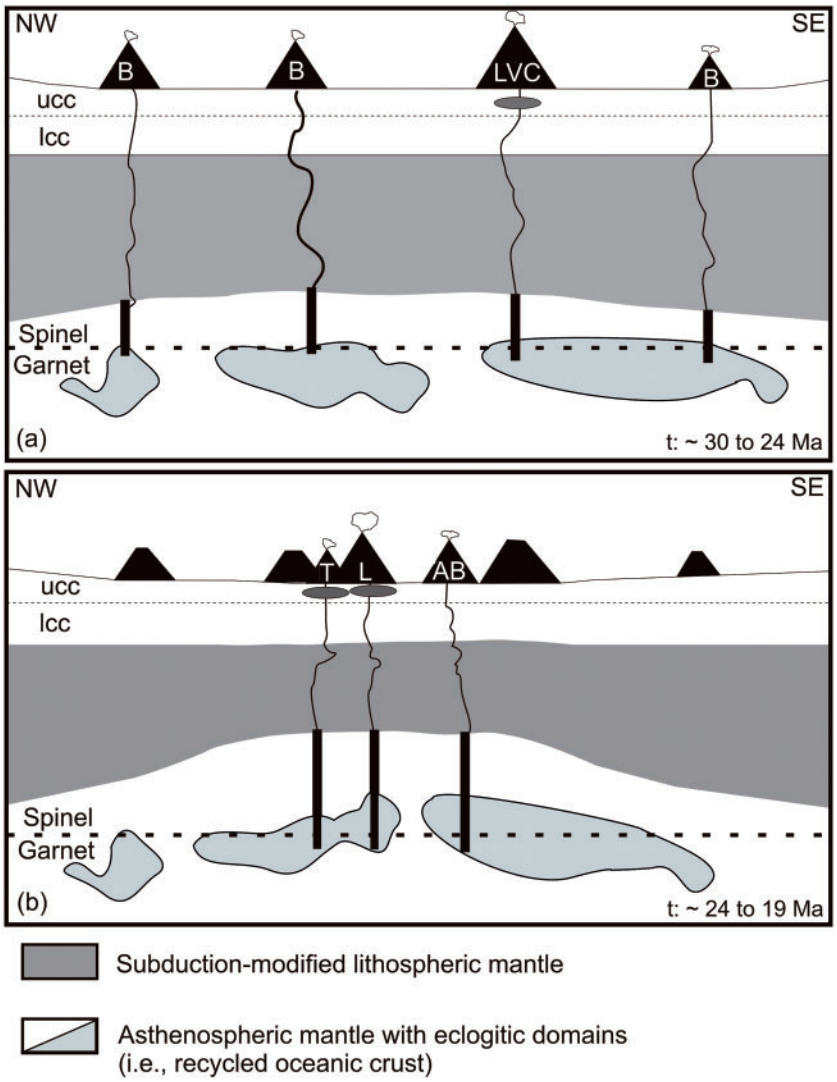

Fig. 11. Schematic sketch illustrating the proposed petrogenetic model for the generation of the SVF magmas. (a) Initial phase of magmatism, formation of basanites (B) and the Löwenburg Volcanic Complex (LVC) above a marginally thinned lithospheric mantle. (b) Continued lithospheric thinning owing to rifting of the Cologne Embayment causes asthenospheric upwelling and reduces the melting depth. Alkali basalts (AB) and their differentiates latite (L) and trachyte (T) are erupted in a NW–SE-trending inner zone. Black rectangles illustrate the different polybaric melting columns; ucc, upper continental crust; lcc, lower continental crust.

Hoernle *et al.*, 1995; Wilson & Patterson, 2001). This view was recently challenged by a model arguing for more passive diapiric upwelling of asthenospheric mantle (Lustrino & Wilson, 2007). Furthermore, the generation of alkaline magmas in response to lithospheric thinning in extensional tectonic regimes is also a viable model applicable to continental rift settings (e.g. McKenzie & Bickle, 1988).

In addition to asthenospheric sources, alkaline mafic magmas could be generated by partial melting of the subcontinental lithospheric mantle (SCLM; e.g. Gallagher & Hawkesworth, 1992; Pilet *et al.*, 2008). This portion of the lithosphere is likely to remain isolated from the convecting upper mantle and thus preserves the imprint of ancient depletion and refertilization events (e.g. Hawkesworth *et al.*, 1990; Pearson & Nowell, 2002). These components then might be able to explain certain isotope characteristics observed in some intraplate lavas (Pilet *et al.*, 2008). Lithospheric mantle xenoliths from the CEVP indeed show substantial trace element and isotopic enrichment linked to subduction zone enrichment during the Variscan orogeny (Witt-Eickschen & Kramm, 1997; Witt-Eickschen *et al.*, 2003).

The mantle sources of the various Cenozoic volcanic fields have been characterized and interpreted in different ways. For the Miocene Vogelsberg shield volcano (18–15 Ma) a temporal evolution from initial magmatism derived

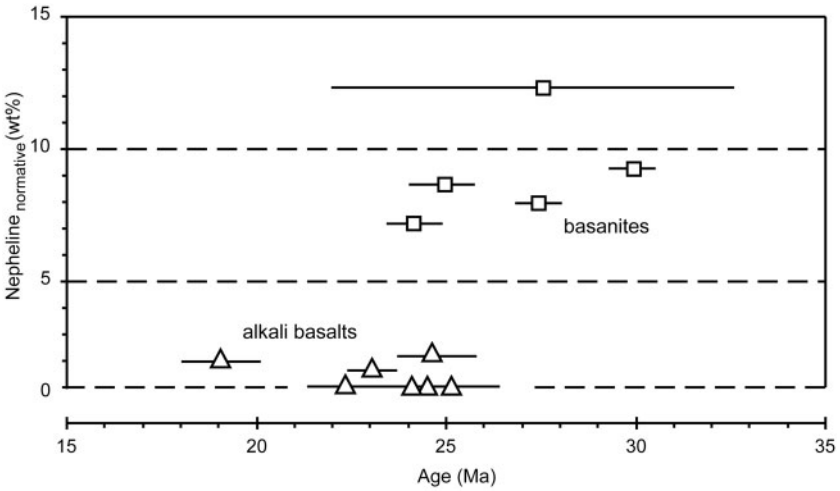

Fig. 12. The degree of SiO_2-undersaturation, indicated by the normative nepheline content of the samples, is highest for lavas erupted early during the evolution of the SVF (30–24 Ma). Alkali basalts erupted during the late phase of SVF activity (25–19 Ma).

from a lithospheric source to a late stage dominated by asthenospheric melts has been proposed (Bogaard & Wörner, 2003). In a similar fashion, Jung *et al.* (2006) suggested a successive change in magma composition for the Hocheifel Volcanic Field (44–34 Ma; Fekiacova *et al.*, 2007*b*), which formed on a block of uplifted basement (Rhenish Massif). Here, it is inferred that interaction of a mantle plume with the overlying mantle lithosphere generated partial melts with an initially high SCLM component, whereas asthenospheric sources dominated during the later stages. For the Westerwald Volcanic Field (30–20 Ma), it has been shown that the magmas were derived from melting of enriched mantle in the garnet stability field, which has also been explained in the context of a mantle plume model (Haase *et al.*, 2004).

Magmatism in the Rhön area and the Hessian Depression is associated with a zone of lithospheric thinning and dextral strike-slip movement that probably caused local passive asthenospheric upwelling (Mengel *et al.* 1983; Wedepohl *et al.* 1983; Wedepohl, 1985; Schreiber & Rotsch, 1998; Wedepohl & Baumann, 1999). Based on Sr–Nd–Pb–Hf–Os isotope systematics, Jung *et al.* (2005, 2011) argued for magma generation in particularly enriched domains at low melting temperatures within a common, depleted asthenospheric upper mantle.

In summary, previous studies have established that the petrogenesis of CEVP magmas involves variable contributions of SCLM components and different asthenospheric mantle sources. There are also different geodynamic scenarios proposed as being responsible for the generation of asthenospheric melts. In areas with prominent basement uplift, such as the Quaternary Eifel, a rising mantle plume may be a convincing model. This is also corroborated by the identification of a finger-like low-velocity anomaly by seismic tomography (Ritter *et al.*, 2001). However, the evidence for mantle plume related material beneath the Paleogene to Neogene volcanic centres is also ambiguous. In contrast to plume models, lithospheric thinning as a result of tectonic stretching and passive upwelling of asthenospheric mantle is a viable alternative scenario that applies in particular to areas such as the Rhön and the Hessian Depression. For the SVF, a link to an extensional tectonic regime is also indicated, as the Rhine Graben dissects the volcanic field. Moreover, the volcanic plugs of the SVF are arranged parallel to the inferred direction of the least tectonic stress component, pointing to a tectonic control on magma ascent pathways.

CONCLUSIONS

A comprehensive major and trace element and Sr–Nd–Pb–Hf isotope dataset for the volcanic rocks of the Siebengebirge Volcanic Field (SVF) allows new insights into the petrogenesis of Cenozoic volcanic rocks in Central Europe. The isotope compositions of the mafic magmas in the SVF point to partial melting of a fairly homogeneous asthenospheric mantle source. This isotope signature is associated with somewhat elevated Zr/Hf ratios, indicating that enriched eclogitic domains (i.e. recycled oceanic crustal material) are also involved. The observed negative K anomalies argue for the presence of lithospheric components, and REE systematics indicate that melting took place mainly in the garnet–spinel transition zone. Basanitic lavas were generated over shorter melting columns and at higher average melting depths than the alkali basalts.

The phonotephritic to tephriphonolitic lavas of the LVC can be related to basanitic parental melts whereas the latites and trachytes formed from alkali basalt parental melts. Energy-constrained AFC modelling (EC-AFC) shows that some mafic lower crustal granulites and mid-crustal metapelites might represent potential

assimilants for the various magma compositions of the LVC. An expanded dataset for the local basement and possible parental melt compositions as well as an improved understanding of ambient pressures and temperatures during the AFC process are clearly required to place tighter constraints on EC-AFC modelling.

We interpret the SVF data in the context of a geodynamic model involving crustal extension during subsidence of the Cologne Embayment along the northern margin of the Paleozoic Rhenish Shield. Initial low-degree melts formed beneath a thick lithospheric mantle lid within particularly fertile domains in the asthenosphere. Basanitic melts were channeled up to the surface following zones of structural weakness at upper crustal levels. This pattern is reflected in the general NW–SE alignment of the relict SVF volcanic edifices. Progressive lithospheric thinning caused further upwelling of the asthenosphere and alkali basaltic magmas formed at higher melting degrees and lower average depths. Available K–Ar and Ar–Ar age data support this model, as basanites erupted first (30–24 Ma) followed by alkali basalts (to 25–19 Ma).

Our case study for the SVF shows that a remarkable diversity of magma compositions may be generated within a single intracontinental volcanic field as a result of changes in melting conditions with time. The compositional evolution towards more felsic magma compositions can be related to enhanced crustal assimilation and fractional crystallization processes. There is a strong link between magmatism and the regional tectonic evolution; namely, crustal thinning and rifting generating the Cologne Embayment. A thermal anomaly, associated with an anomalously hot mantle plume, is not necessarily required to explain the SVF magmatism.

ACKNOWLEDGEMENTS

Our study greatly benefited from the collection of Siebengebirge samples and previous data that K. Vieten kindly made available. R. Hoffbauer (University of Bonn, XRF) and D. Garbe-Schönberg (University Kiel, ICP-MS analyses) provided major and trace element data. H. Baier is thanked for advice and assistance during isotope measurements at Universität Münster. Helpful discussions and laboratory access by K. Mezger (Universität Münster) are acknowledged. M. Valdivia-Manchego (University of Bonn) is thanked for providing assistance with using the Surfer software (Version 8.0) for contouring normative nepheline contents of the SVF volcanic rocks. The paper benefited from comments by S. Schuth, who reviewed an early version of the paper, and detailed reviews by G. Fitton, K. Haase and two anonymous reviewers.

SUPPLEMENTARY DATA

Supplementary data for this paper are available at *Journal of Petrology* online.

REFERENCES

Albarède, F., Télouk, P., Blichert-Toft, J., Boyet, M., Agranier, A. & Nelson, B. (2004). Precise and accurate isotopic measurements using multiple-collector ICPMS. *Geochimica et Cosmochimica Acta* **68**, 2725–2744.

Anderson, D. L. (2011). Hawaii, boundary layers and ambient mantle—geophysical constraints. *Journal of Petrology* **52**, 1547–1577.

Babuska, V. & Plomerova, J. (1992). The lithosphere in Central Europe—seismological and petrological aspects. *Tectonophysics* **207**, 101–163.

Bizimis, M., Salters, V. J. M. & Dawson, J. B. (2003). The brevity of carbonatite sources in the mantle: evidence from Hf isotopes. *Contribution to Mineralogy and Petrology* **145**, 281–300.

Blichert-Toft, J. & Albarède, F. (1997). The Lu–Hf isotope geochemistry of chondrites and the evolution of the mantle–crust system. *Earth and Planetary Science Letters* **148**, 243–258.

Blundy, J. D., Robinson, J. A. C. & Wood, B. J. (1998). Heavy REE are compatible in clinopyroxene on the spinel lherzolite solidus. *Earth and Planetary Science Letters* **160**, 493–504.

Blusztajn, J. & Hegner, E. (2002). Osmium isotopic systematics of melilities from the Tertiary Central European Volcanic province in SW Germany. *Chemical Geology* **189**, 91–103.

Bogaard, P. J. F. & Wörner, G. (2003). Petrogenesis of basanitic to tholeiitic volcanic rocks from the Miocene Vogelsberg, Central Germany. *Journal of Petrology* **44**, 569–602.

Bohrson, W. A. & Spera, F. J. (2001). Energy-constrained open-system magmatic processes II: application of energy-constrained assimilation–fractional crystallization (EC-AFC) model to magmatic systems. *Journal of Petrology* 1019–1041.

Boynton, W. V. (1984). Cosmochemistry of the rare earth elements: meteorite studies. In: Henderson, P. (ed.) *Rare Earth Element Geochemistry*. Amsterdam: Elsevier, pp. 89–94.

Cebriá, J. M. & Wilson, M. (1995). Cenozoic mafic magmatism in Central Europe: a common European Asthenospheric Reservoir? *Terra Abstracts* **7**, 162.

Class, C. & Goldstein, S. L. (1997). Plume–lithosphere interactions in the ocean basins: constraints from the source mineralogy. *Earth and Planetary Science Letters* **150**, 245–260.

Dasgupta, R., Hirschmann, M. M. & Smith, N. D. (2007). Partial melting experiments of peridotite + CO_2 at 3 GPa and genesis of alkalic ocean island basalts. *Journal of Petrology* **48**, 2093–2124.

David, K., Schiano, P. & Allègre, C. J. (2000). Assessment of the Zr/Hf fractionation in oceanic basalts and continental materials during petrogenetic processes. *Earth and Planetary Science Letters* **178**, 285–301.

Drake, M. J. (1975). The oxidation state of europium as an indicator of oxygen fugacity. *Geochimica et Cosmochimica Acta* **39**, 55–64.

Duda, A. & Schmincke, H. U. (1985). Polybaric differentiation of alkali basaltic magmas: evidence from green-core clinopyroxenes 95 (Eifel, FRG). *Contributions to Mineralogy and Petrology* **91**, 340–353.

Dunworth, E. A. & Wilson, M. (1998). Olivine melilites of the SW German Tertiary volcanic province: Mineralogy and petrogenesis. *Journal of Petrology* **39**, 1805–1836.

Dupuy, C., Liotard, J. M. & Dostal, J. (1992). Zr/Hf fractionation in intraplate basaltic rocks—carbonate metasomatism in the mantle source. *Geochimica et Cosmochimica Acta* **56**, 2417–2423.

Fekiakova, Z., Mertz, D. F. & Hofmann, A. W. (2007*a*). Geodynamic setting of the Tertiary Hocheifel volcanism (Germany), Part II: Geochemistry and Sr, Nd and Pb isotopic compositions. In: Ritter, J. R. R. & Christensen, U. R. (eds) *Mantle plumes – a multidisciplinary approach*. Heidelberg: Springer, pp. 207–240.

Fekiacova, Z., Mertz, D. F. & Renne, P. R. (2007*b*). Geodynamic setting of the Tertiary Hocheifel volcanism (Germany), Part I: 40Ar/39Ar geochronology. In: Ritter, J. R. R. & Christensen, U. R. (eds) *Mantle Plumes—a Multidisciplinary Approach*. Heidelberg: Springer, pp. 185–206.

Foley, S. F. (1992). Vein-plus-wallrock melting mechanisms in the lithosphere and the origin of potassic alkaline magmas. *Lithos* **28**, 435–453.

Frechen, J. & Vieten, K. (1970*a*). Petrographie der Vulkanite des Siebengebirges. Die peralkalische Gesteinsreihe Alkalitrachyt–Sanidinbasanit. *Decheniana* **122**, 357–377.

Frechen, J. & Vieten, K. (1970*b*). Petrographie der Vulkanite des Siebengebirges. Die subalkalische Gesteinsreihe Quarztrachyt–Latitbasalt. *Decheniana* **122**, 337–356.

Frey, F. A., Green, D. H. & Roy, S. D. (1978). Integrated models of basalt petrogenesis: A study of quartz tholeiites to olivine melilitites from South Eastern Australia utilizing geochemical and experimental petrological data. *Journal of Petrology* **19**, 463–513.

Furman, T. (1995). Melting of metasomatized subcontinental lithosphere—undersaturated mafic lavas from Rungwe, Tanzania. *Contributions to Mineralogy and Petrology* **122**, 97–115.

Galer, S. J. G. & Abouchami, W. (1998). Practical application of lead triple spiking for correction of instrumental mass discrimination. *Mineralogical Magazine* **62A**, 491–492.

Gallagher, K. & Hawkesworth, C. J. (1992). Dehydration melting and the generation of continental flood basalts. *Nature* **358**, 57–59.

Goes, S., Spakman, W. & Bijqaard, H. (1999). A lower mantle source for central European volcanism. *Science* **286**, 1928–1931.

Garbe-Schönberg, C. D. (1993). Simultaneous determination of 37 trace elements in 28 international rock standards by ICP-MS. *Geostandards Newsletter* **17**, 81–93.

Govindaraju, K. (1994). Compilation of working values and sample description for 383 geostandards. *Geostandards Newsletter* **18**, 1–158.

Granet, M., Wilson, M. & Achauer, U. (1995). Imaging a mantle plume beneath the French Massif Central. *Earth and Planetary Science Letters* **136**, 281–296.

Green, D. H. & Ringwood, A. E. (1967). The stability fields of aluminous pyroxene peridotite and garnet peridotite and their relevance in upper mantle structure. *Earth and Planetary Science Letters* **3**, 151–160.

Green, T. H., Blundy, J. D., Adam, J. & Yaxley, G. M. (2000). SIMS determination of trace element partition coefficients between garnet, clinopyroxene and hydrous basaltic liquids at 2–7·5 GPa and 1080–1200°C. *Lithos* **53**, 165–187.

Grégoire, M., Bell, D. R. & Le Roex, A. P. (2002). Trace element geochemistry of phlogopite-rich mafic mantle xenoliths: their classification and their relationship to phlogopite-bearing peridotites and kimberlites revisited. *Contributions to Mineralogy and Petrology* **142**, 603–625.

Haase, K. M. & Renno, A. D. (2008). Variation of magma generation and mantle sources during continental rifting observed in Cenozoic lavas from the Eger rift, Central Europe. *Chemical Geology* **257**, 195–205.

Haase, K. M., Goldschmidt, B. & Garbe-Schönberg, C.-D. (2004). Petrogenesis of Tertiary continental intra-plate lavas from the Westerwald region, Germany. *Journal of Petrology* **45**, 883–905.

Hall, R. & Spakman, W. (2002). Subducted slabs beneath the eastern Indonesia–Tonga region: insights from tomography. *Earth and Planetary Science Letters* **201**, 321–336.

Hart, S. R., Hauri, E. H., Oschmann, L. A. & Whitehead, J. A. (1992). Mantle plumes and entrainment: Isotopic evidence. *Science* **256**, 517–520.

Hartmann, G. & Wedepohl, K. H. (1990). Metasomatically altered peridotite xenoliths from the Hessian Depression (Northwest Germany). *Geochimica et Cosmochimica Acta* **54**, 71–86.

Hawkesworth, C. J., Kempton, P. D., Rogers, N. W., Ellam, R. M. & Van Calsteren, P. W. (1990). Continental mantle lithosphere, and shallow level enrichment in the Earth's mantle. *Earth and Planetary Science Letters* **96**, 256–268.

Hegner, E., Walter, H. J. & Satir, M. (1995). Pb–Sr–Nd isotopic compositions and trace element geochemistry of megacrysts and melilites from the Tertiary Urach volcanic field: source composition of small volume melts under SW Germany. *Contributions to Mineralogy and Petrology* **122**, 322–335.

Herzberg, C. (1995). Generation of plume magmas through time: an experimental perspective. *Chemical Geology* **126**, 1–16.

Hirata, T. (1996). Lead isotopic analyses of NIST standard reference material using multiple collector inductively coupled plasma mass spectrometry coupled with a modified external correction method for mass discrimination effect. *Analyst* **121**, 1407–1411.

Hirschmann, M. M., Kogiso, T., Baker, M. B. & Stolper, E. M. (2003). Alkalic magmas generated by partial melting of garnet pyroxenite. *Geology* **31**, 481–484.

Hoernle, K., Zhang, Y. S. & Graham, D. (1995). Seismic and geochemical evidence for large-scale mantle upwelling beneath the eastern Atlantic and western and Central Europe. *Nature* **374**, 34–39.

Hofmann, A. W. (1997). Mantle geochemistry: the message from oceanic volcanism. *Nature* **385**, 219–229.

Hofmann, A. W. (2003). Sampling mantle heterogeneity through ocean basalts: Isotope and trace elements. In: Holland, H. D. & Turekian, K. K. (eds) *Treatise on Geochemistry Volume 2: The Mantle and Core*. Amsterdam: Elsevier, pp. 61–101.

Hofmann, A. W. & White, M. W. (1982). Mantle plumes from ancient oceanic crust. *Earth and Planetary Science Letters* **79**, 33–45.

Jung, C., Jung, S., Hoffer, E. & Berndt, J. (2006). Petrogenesis of Tertiary mafic alkaline magmas in the Hocheifel, Germany. *Journal of Petrology* **47**, 1637–1671.

Jung, S. & Hoernes, S. (2000). The major- and trace-element and isotope (Sr, Nd, O) geochemistry of Cenozoic alkaline rift-type volcanic rocks from the Rhön area (Central Germany): petrology, mantle source characteristics and implications for asthenosphere–lithosphere interactions. *Journal of Volcanology and Geothermal Research* **99**, 27–53.

Jung, S. & Masberg, P. (1998). Major- and trace-element systematics and isotope geochemistry of Cenozoic mafic volcanic rocks from the Vogelsberg (central Germany): Constraints on the origin of continental alkaline and tholeiitic basalts and their mantle sources. *Journal of Volcanology and Geothermal Research* **86**, 151–177.

Jung, S., Pfänder, J. A., Brügmann, G. & Stracke, A. (2005). Sources of primitive alkaline volcanic rocks from the Central European volcanic province (Rhön, Germany) inferred from Hf, Os and Pb isotopes. *Contributions to Mineralogy and Petrology* **150**, 546–559.

Jung, S., Pfänder, J. A., Brauns, M. & Maas, R. (2011). Crustal contamination and mantle source characteristics in continental intra-plate volcanic rocks: Pb, Hf and Os isotopes from central European volcanic province basalts. *Geochimica et Cosmochimica Acta* **75**, 2664–2683.

Klemme, S., Blundy, J. D. & Wood, B. J. (2002). Experimental constraints on major and trace element partitioning during partial melting of eclogite. *Geochimica et Cosmochimica Acta* **66**, 3109–3123.

Kogiso, T. & Hirschmann, M. M. (2001). Experimental study of clinopyroxenite partial melting and the origin of ultra-calcic melt inclusions. *Contributions to Mineralogy and Petrology* **142**, 347–360.

Kogiso, T., Hirschmann, M. M. & Frost, D. J. (2003). High-pressure partial melting of garnet pyroxenite: possible mafic lithologies in

the source of ocean island basalts. *Earth and Planetary Science Letters* **216**, 603–617.

Korkisch, J. & Hazan, I. (1965). Anion exchange separations in hydrobromic acid–organic solvent media. *Analytical Chemistry* **37**, 707–710.

Kramm, U. & Wedepohl, K. H. (1990). Tertiary basalts and peridotite xenoliths from the Hessian Depression (NW Germany), reflecting mantle compositions low in radiogenic Nd and Sr. *Contributions to Mineralogy and Petrology* **106**, 1–8.

Langmuir, C. H., Klein, E. M. & Plank, T. (1992). Petrological systematics of mid-ocean ridge basalts: constraints on melt generation beneath ocean ridges. In: Morgan, J. P., Blackman, D. K. & Sinton, J. M. (eds) *Mantle Flow and Melt Generation at Mid-ocean Ridges. Geophysical Monograph, American Geophysical Union* **71**, 183–280.

Le Maitre, R. W. (2002). *A Classification and Glossary of Terms: Recommendations of the International Union of Geological Sciences Subcommission on the Systematics of Igneous Rocks*. Cambridge: Cambridge University Press.

Le Roex, A. P., Späth, A. & Zartman, R. E. (2001). Lithospheric thickness beneath the southern Kenya Rift: implications from basalt geochemistry. *Contributions to Mineralogy and Petrology* **142**, 89–106.

Linthout, K., Paulick, H. & Wijbrans, J. R. (2009). Provenance of basalt blocks from Roman sites in Vleuten-De Meern (The Netherlands) traced to the Tertiary Siebengebirge (Germany): A geoarcheological quest using petrological and geochemical methods. *Geologie en Mijnbouw* **88**, 78–99.

Loock, G., Stosch, H. G. & Seck, H. A. (1990). Granulite facies lower crustal xenoliths from the Eifel, West Germany: petrological and geochemical aspects. *Contributions to Mineralogy and Petrology* **105.**

Lustrino, M. (2011). What 'anorogenic' igneous rocks can tell us about the chemical composition of the upper mantle: case studies from the circum-Mediterranean area. *Geological Magazine* **148**, 304–316.

Lustrino, M. & Wilson, M. (2007). The circum-Mediterranean anorogenic Cenozoic igneous province. *Earth-Science Reviews* **81**, 1–65.

McDonough, W. F. & Sun, S.-s. (1995). The composition of the Earth. *Chemical Geology* **120**, 223–253.

McKenzie, D. & Bickle, M. J. (1988). The volume and composition of melt generated by extension of the lithosphere. *Journal of Petrology* **29**, 625–679.

Mengel, K., Kramm, U., Wedepohl, K. H. & Gohn, E. (1983). Sr-isotope of Miocene basalt and peridotite pockets of Northern Hessian Depressions. *Fortschritte der Mineralogie* **61**, 147–149.

Metzner, C. (1983). *Petrographie und Petrochemie von Latiten der Tertiären Alkalibasalt–Trachyt Assoziation des Siebengebirges*, Diploma thesis, University of Bonn, 76 pp.

Münker, C., Weyer, S., Scherer, E. & Mezger, K. (2001). Separation of high field strength elements (Nb, Ta, Zr, Hf) and Lu from rock samples for MC-ICP-MS measurements. *Geochemistry, Geophysics, Geosystems* **2**, 2001GC00183.

Münker, C., Pfänder, J. A., Weyer, S., Büchl, A., Kleine, T. & Mezger, K. (2003). Evolution of planetary cores and the Earth–Moon system from Nb/Ta systematics. *Science* **301**, 84–87.

Oncken, O., Winterfeld, C. & Dittmar, U. (1999). Accretion and inversion of a rifted passive margin—the late Paleozoic Rhenohercynian fold and thrust belt. *Tectonics* **18**, 75–91.

Pearson, D. G. & Nowell, G. M. (2002). The continental lithospheric mantle: characteristics and significance as a mantle reservoir. *Philosophical Transactions of the Royal Society of London, Series A* **360**, 2383–2410.

Pertermann, M. & Hirschmann, M. M. (2003). Anhydrous partial melting experiments on MORB-like eclogite: Phase relations, phase compositions and mineral–melt partitioning of major elements at 2–3 GPa. *Journal of Petrology* **44**, 2173–2201.

Petrelli, M., Poli, G., Perugini, D. & Peccerillo, A. (2005). PetroGraph: A new software to visualize, model, and present geochemical data in igneous petrology. *Geochemistry, Geophysics, Geosystems* , doi:10.1029/2005GC000932.

Pfänder, J. A., Munker, C., Stracke, A. & Mezger, K. (2007). Nb/Ta and Zr/Hf in ocean island basalts—Implications for crust–mantle differentiation and the fate of niobium. *Earth and Planetary Science Letters* **254**, 158–172.

Pfänder, J. A., Jung, S., Münker, C., Stracke, A. & Mezger, K. (2012). A possible high Nb/Ta reservoir in the continental lithospheric mantle and consequences on the global Nb budget—Evidence from continental basalts from Central Germany. *Geochimica et Cosmochimica Acta* **77**, 232–251.

Pilet, S., Baker, M. B. & Stolper, E. M. (2008). Metasomatized lithosphere and the origin of alkaline lavas. *Science* **320**, 916–919.

Prodehl, C. (1981). Structure of the crust and upper mantle beneath the Central European rift system. *Tectonophysics* **80**, 255–269.

Prodehl, C., Mueller, S., Glahn, A., Gutscher, M. & Haak, V. (1992). Lithospheric cross sections of the European Cenozoic rift system. *Tectonophysics* **208**, 113–138.

Rehkämper, M. & Halliday, A. M. (1998). Accuracy and long-term reproducibility of lead isotopic measurements by MC-ICP-MS using an external method for correction of mass discrimination. *International Journal of Mass Spectrometry and Ion Processes* **58**, 123–133.

Ritter, J. R. R., Jordan, M., Christensen, U. R. & Achauer, U. (2001). A mantle plume beneath the Eifel volcanic fields, Germany. *Earth and Planetary Science Letters* **186**, 7–14.

Robinson, J. A. C. & Wood, B. J. (1998). The depth of the spinel to garnet transition at the peridotite solidus. *Earth and Planetary Science Letters* **164**, 277–284.

Rosenbaum, J. M. & Wilson, M. (1996). Two-stage enrichment of the Eifel mantle: new evidence. *Journal of Conference Abstracts* **1**, 523.

Rudnick, R. L. & Goldstein, S. L. (1990). The Pb isotopic composition of lower crustal xenoliths and the evolution of lower crustal Pb. *Earth and Planetary Science Letters* **98**, 192–207.

Schreiber, U. & Rotsch, S. (1998). Cenozoic block rotation according to conjugate shear system in Central Europe—indications from paleomagnetic measurements. *Tectonophysics* **299**, 111–142.

Schuth, S., König, S. & Münker, C. (2011). Subduction zone dynamics in the SW Pacific plate boundary region constrained from high-precision Pb isotope data. *Earth and Planetary Science Letters* **311(3–4)**, 328–338.

Späth, A., Le Roex, A. P. & Opiyo-Akech, N. (2001). Plume–lithosphere interaction and the origin of continental rift related alkaline volcanism—the Chyulu Hill volcanic province, southern Kenya. *Journal of Petrology* **42**, 765–787.

Spera, F. J. & Bohrson, W. A. (2001). Energy-constrained open-system magmatic processes I: general model and energy-constrained assimilation and fractional crystallization (EC-AFC) formulation. *Journal of Petrology* **42**, 999–1018.

Stosch, H. G. & Lugmair, G. W. (1984). Evolution of lower continental crust: granulite facies xenoliths from the Eifel, West Germany. *Nature* **311**, 368–370.

Stosch, H. G. & Lugmair, G. W. (1986). Trace element and Sr and Nd isotope geochemistry of peridotite xenoliths from the Eifel (West Germany) and their bearing on the evolution of the sublithosphere. *Earth and Planetary Science Letters* **80**, 281–298.

Stosch, H. G. & Seck, H. A. (1980). Geochemistry and mineralogy of 2 spinel peridotite from Dreiser-Weiher, West Germany. *Geochimica et Cosmochimica Acta* **44**, 457–470.

Stosch, H. G., Schmucker, A. & Reys, C. (1991). The nature and geological history of the deep crust under the Eifel, Germany. *Terra Nova* **4**, 53–62.

Stracke, A., Hofmann, A. W. & Hart, S. R. (2005). FOZO, HIMU and the rest of the mantle zoo. *Geochemistry, Geophysics, Geosystems* **6**, Q05007, doi:10.1029/2004GC00824.

Todt, W. & Lippolt, H. J. (1980). K–Ar age determination on tertiary volcanic rocks: V. Siebengebirge, Siebengebirge-Graben. *Journal of Geophysics* **48**, 18–27.

Ulrych, J., Dostal., J., Adamovic, J., Jelinek, E., Spacek, P., Hegner, E. & Balogh, K. (2011). Recurrent Cenozoic volcanic activity in the Bohemian Massif (Czech Republic). *Lithos* **123**, 133–144.

van Westrenen, W., Blundy, J. D. & Wood, B. J. (2001*a*). High field strength element/rare earth element fractionation during partial melting in the presence of garnet: implications for identification of mantle heterogeneities. *Geochemistry, Geophysics, Geosystems* **2**, 200GC000133.

van Westrenen, W., Wood, B. J. & Blundy, J. D. (2001*b*). A predictive thermodynamic model of garnet–melt trace element partitioning. *Contributions to Mineralogy and Petrology* **142**, 219–234.

Vervoort, J. D., Patchett, J. P., Blichert-Toft, J. & Albarède, F. (1999). Relationships between Lu–Hf and Sm–Nd isotopic systems in the global sedimentary system. *Earth and Planetary Science Letters* **168**, 79–99.

Vieten, K. (1983). Tertiary volcanism in the Siebengebirge mountains. In: Fuchs, K., von Gehlen, K., Mälzer, H., Murawski, H. & Semmel, A. (eds) *Plateau Uplift—The Rhenish Shield—A Case History*. Berlin: Springer, pp. 131–132.

Vieten, K. (1987). *Abschlussbericht an die Deutsche Forschungsgemeinschaft zum Projekt: Raum-Stoff-Plan der tertiären Alkalibasalte in der nördlichen Mittelrhein-Region (VI-75/3)*. Bonn: University of Bonn, pp. 1–99.

Vieten, K., Hamm, H. M. & Grimmeisen, W. (1988). Tertiärer Vulkanismus des Siebengebirges. *Fortschritte der Mineralogie, Beihefte* **66**, 1–42.

Wallace, M. E. & Green, D. H. (1991). The effect of bulk rock composition on the stability of amphibole in the upper mantle: Implications for solidus positions and mantle metasomatism. *Mineralogy and Petrology* **44**, 1–19.

Walter, M. J. (1998). Melting of garnet peridotite and the origin of komatiite and depleted lithosphere. *Journal of Petrology* **39**, 29–60.

Wasserburg, G. J., Jacobsen, S. B., De Paolo, D. J., McCulloch, M. T. & Wen, T. (1981). Precise determination of Sm/Nd ratios, Sm and Nd isotopic abundances in standard solutions. *Geochimica et Cosmochimica Acta* **45**, 2311–2323.

Wedepohl, K. H. (1985). Origin of the Tertiary basaltic volcanism in the Northern Hessian Depression. *Contributions to Mineralogy and Petrology* **89**, 122–143.

Wedepohl, K. H. (2000). The composition and formation of Miocene tholeiites in the Central European Cenozoic plume volcanism (CECV). *Contributions to Mineralogy and Petrology* **140**, 180–189.

Wedepohl, K. H. & Baumann, A. (1999). Central European Cenozoic plume volcanism with OIB characteristics and indications of lower mantle source. *Contributions to Mineralogy and Petrology* **136**, 225–239.

Wedepohl, K. H., Mengel, K. & Ritzkowski, S. (1983). The Tertiary basalts of the Northern Hessian Depression and their mantle xenoliths. *Fortschritte der Mineralogie* **61**, 117–134.

Wedepohl, K. H., Gohn, E. & Hartmann, G. (1994). Cenozoic alkali basaltic magmas of western Germany and their products of differentiation. *Contributions to Mineralogy and Petrology* **115**, 253–278.

Weill, D. F. & Drake, M. J. (1973). Europium anomaly in plagioclase feldspar: experimental results and semiquantitative model. *Science* **180**, 1059–1060.

Wilson, M. & Downes, H. (1991). Tertiary–Quaternary extension-related alkaline magmatism in Western and Central Europe. *Journal of Petrology* **32**, 811–849.

Wilson, M. & Downes, H. (2006). Tertiary–Quaternary intra-plate magmatism in Europe and its relationship to mantle dynamics. In: Gee, D. & Stephenson, R. A. (eds) *European Lithosphere Dynamics. Geological Society, London, Memoirs* **32**, 147–166.

Wilson, M. & Patterson, R. (2001). Intra-plate magmatism related to hot fingers in the upper mantle: evidence from the Tertiary–Quaternary volcanic province of western and central Europe. In: Ernst, R. & Buchan, K. (eds) *Mantle Plumes: their Identification through Time. Geological Society of America, Special Papers* **352**, 37–58.

Wilson, M., Rosenbaum, J. M. & Dunworth, E. A. (1995). Melilitites: partial melts of the thermal boundary layer? *Contributions to Mineralogy and Petrology* **119**, 181–196.

Witt-Eickschen, G. & Kramm, U. (1997). Mantle upwelling and metasomatism beneath Central Europe: Geochemical and isotopic constraints from mantle xenoliths from the Rhön (Germany). *Journal of Petrology* **38**, 479–493.

Witt-Eickschen, G., Kaminsky, W., Kramm, U. & Harte, B. (1998). The nature of young vein metasomatism in the lithosphere of the West Eifel (Germany): geochemical and isotopic constraints from composite mantle xenoliths from the Meerfelder Maar. *Journal of Petrology* **39**, 155–185.

Witt-Eickschen, G., Seck, H. A., Mezger, K., Eggins, S. M. & Altherr, R. (2003). Lithospheric mantle evolution beneath the Eifel (Germany): Constraints from Sr–Nd–Pb isotopes and trace element abundances in spinel peridotite and pyroxenite veins. *Journal of Petrology* **44**, 1077–1095.

Wittenbecher, M. (1992). Geochemie tholeiitischer und alkali-olivinbasaltischer Gesteine des Vogelsberges. *Geologische Abhandlungen Hessen* **97**, 3–52.

Wörner, G., Schmincke, H. U. & Schreyer, W. (1982). Crustal xenoliths from the Quaternary Wehr volcano (East Eifel). *Neues Jahrbuch für Mineralogie, Abhandlungen* **144**, 29–35.

Wörner, G., Staudigel, H. & Zindler, A. (1985). Isotopic constraints on open system evolution of the Laacher See magma chamber (Eifel, West Germany). *Earth and Planetary Science Letters* **75**, 37–49.

Wörner, G., Zindler, A., Staudigel, H. & Schmincke, H. U. (1986). Sr, Nd, and Pb isotope geochemistry of Tertiary and Quaternary alkaline volcanics from West Germany. *Earth and Planetary Science Letters* **79**, 107–119.

Ziegler, P. A. (1992). European Cenozoic rift system. *Tectonophysics* **208**, 91–111.